Medium Range Prediction by a GFDL Global Spectral Model: Results for Three Winter Cases and Sensitivity to Dissipation

CHARLES T. GORDON AND WILLIAM F. STERN

Geophysical Fluid Dynamics Laboratory/NOAA, Princeton University, Princeton, NJ 08542

(Manuscript received 26 February 1983, in final form 26 September 1983)

ABSTRACT

A preliminary evaluation is made of the medium range predictive capability of a GFDL global spectral model of the atmosphere, based upon three winter blocking cases. Analogous forecasts by a GFDL global grid point model provide a background standard of comparison. The spectral model is rhomboidally truncated at wavenumber 30, has 9 sigma levels, incorporates sub-grid scale physical processes commonly associated with general circulation models and employs semi-implicit time differencing. The grid point model has somewhat finer horizontal resolution and fairly similar sub-grid scale physical processes, and employs explicit time differencing. The spectral model is up to 6 times more economical.

The level of forecast skill for the 5 to 15 day range is generally less than practically useful and is more case-dependent than spectral versus grid point model-dependent. In the most successful case, i.e., 16 January 1979, an observed Atlantic blocking ridge is simulated quite well, especially by the spectral model. The predicted Atlantic ridges tend to retard approaching upstream transient disturbances. A zonal bias of the midlatitude circulation, which develops in all three spectral and grid point model predictions is most pronounced in the spectral model forecast from 1 January 1977.

Results of a diffusion sensitivity experiment and other evidence suggest that insufficient frictional dissipation may have enhanced the zonal bias of the above forecast. The bias diminishes, consistent with a redistribution of spectral kinetic energy among zonal wavenumbers 0, 1 and 2, if a static stability-dependent parameterization of vertical mixing or stronger ∇^4 horizontal diffusion are used. Also, the predicted-enstrophy spectrum at midlatitudes steepens, given the stronger ∇^4 horizontal diffusion.

1. Introduction

Considerable attention has been focused during the past decade on medium range numerical weather prediction. Not only is this forecast range of intrinsic interest. But, in addition, the results could provide guidance for the development of long-range prediction models. Miyakoda, *et al.* (1972; 1979) demonstrated the feasibility of medium range numerical prediction, using a hemispheric, 2.25° resolution, 9 level grid point model. Their predicted large-scale geopotential height field retained limited but detectable skill beyond 10 days at 500 mb and 5 days at 1000 mb. Meanwhile, some impressive medium range prediction models have been developed at the European Centre for Medium Range Weather Forecasts (ECMWF). A global, 1.875° resolution, 15 level grid point model is currently being integrated out to 10 days on an operational basis. According to Hollingsworth *et al.* (1980), its forecasts have practically useful skill for 5 to 6 days. Furthermore, using a spectral model, triangularly truncated at wave number 63, this range can be extended by 6 to 9 hours, according to Jarraud *et al.* (1981).

The success of the above prediction models is related to their moderately high spatial resolution and to adequate physical processes of the type found in general circulation models (GCMs). From a practical standpoint, an extended range prediction model must also be computationally efficient.

With the above requirements in mind, a global spectral prediction model with orography, land–sea contrast, moist processes, dry and moist convective adjustment, radiative transfer and horizontal and vertical sub-grid scale mixing has been developed at the Geophysical Fluid Dynamics Laboratory (GFDL). A detailed documentation may be found in Gordon and Stern (1982, hereafter referred to as GS). The standard version, i.e., R30L09 is rhomboidally truncated at wave number 30, has 9 sigma levels, utilizes leapfrog semi-implicit time differencing and incorporates the so-called "A" physics parameterization of sub-grid scale vertical turbulent mixing. In the surface boundary layer, vertical diffusion is governed by bulk aerodynamic drag laws. Within the planetary boundary layer, the diffusion of momentum and water vapor is based on Prandtl mixing length theory for a neutrally stratified atmosphere. The more advanced "E4" physics (see GS or Section 5) has been implemented as a spectral model option.

The main objective of the present paper is to provide a preliminary assessment of the medium range predictive capability of the GFDL R30L09 global spectral

model. Forecasts for three winter cases are verified against observation with emphasis on the 5 to 15 day range. Analogous forecasts by a GFDL N48L09 grid point model, with somewhat finer horizontal resolution and similar but not identical sub-grid scale physical processes, provide a background standard of comparison.

A second objective is to examine the possibility that insufficient frictional dissipation enhances the zonal bias of the predicted midlatitude circulation. For this purpose, a prognostic diffusion sensitivity experiment is performed. Also, the dissipation rates of the observed January 1977 monthly mean vorticity and temperature fields are diagnosed for four different diffusion schemes.

2. Preliminary considerations

a. Selection of cases

The basic comparison between the R30L09 spectral versus the N48L09 grid point model forecasts is limited to three winter blocking cases, i.e., 1 March 1965, 1 January 1977 and 16 January 1979. The decision to concentrate on a few cases was influenced mainly by the computational requirements (150 minutes of cpu time per model day) of the N48L09 model. Such a strategy has been exploited, for example, by Miyakoda *et al.* (1983). Of course, many more cases would be needed to establish statistical validity, even for the subpopulation of winter blocking cases. Also, the three sets of initial conditions may not be comparable in quality because the data network and analyses procedures have improved since 1965 and 16 January 1979 falls within the first special observing period of the First GARP Global Experiment (FGGE).

b. Inter-model differences

The R30L09 A spectral and N48L09 A grid point models possess similar but not identical sub-grid scale physics, different time differencing schemes and somewhat different horizontal resolution. These differences are *extrinsic* to the spectral versus finite difference method. With the exception of horizontal resolution, they are summarized in Table 1. Model updates which were made after the completion of the 1 March 1965 integrations are also listed. Note that "A2" physics is the same as "A1", except that in "A2": the surface drag coefficient includes land–sea contrast, the surface temperature over sea ice is determined from a surface heat balance calculation instead of being fixed, and the surface albedo over snow-free land is longitude-dependent. The two radiation schemes and the modified economical explicit time differencing schemes are based upon Manabe and Strickler (1964), Fels and Schwarzkopf (1975) and Brown and Campana (1978), respectively.

The differences in Table 1 which pertain to horizontal diffusion are probably the most important. In all three integrations, the grid point model employed nonlinear horizontal diffusion, whereas the spectral model employed a linear ∇^4 scheme. Moreover, after the R30L09 integration for the case of 1 March 1965 was completed, the ∇^4 horizontal diffusion coefficient was reduced to 2.68×10^{15} m^4 s^{-1} for the case of 1 January 1977, then increased to 1.0×10^{16} m^4 s^{-1} for the case of 16 January 1979.

The difference in effective resolution of the R30 spectral and N48 grid point models is potentially important, although its impact is not investigated here. In the N48 model, the meridional increment is $\Delta\varphi \sim 1.875°$, corresponding to 48 grid points between the equator and either pole. Also, the model's longitudinal increment $\Delta\lambda$ decreases from $5° \leqslant \Delta\lambda \leqslant 10°$ at polar latitudes to $\leqslant 3°$ at midlatitudes to 1.875° in the tropics, since a modified Kurihara grid (Kurihara, 1965; Umscheid and Sankar-Rao, 1971) is used. The estimation of the spectral model's nominal grid resolution is less straightforward. One possible measure is the grid increment which just resolves the Nyquist mode, i.e., cutoff wavenumber (2 grid points per wavelength). But a more relevant measure may be the resolution of the coarsest transform grid which prevents aliasing of the quadratic terms. The longitudinal and meridional grid increments then correspond to approximately 3 and 2.5 grid points, respectively, per wavelength of the Nyquist mode. But using even this more optimistic estimate, $\Delta\lambda \sim 4.0°$ and $\Delta\varphi \sim 2.4°$ for the R30L09 spectral model. Thus, this model appears to have somewhat coarser horizontal resolution at middle latitudes and especially in the tropics, compared to the N48L09 grid point model. A recently developed R42L09 global spectral model is a more equal match for the N48 with respect to resolution.

Other inter-model differences such as semi-implicit versus explicit time differencing or Fels–Schwarzkopf versus Manabe–Strickler radiation appear to be relatively unimportant out to 10 days. This very tentative conclusion is based upon some sensitivity tests (pairs of 10 day R21L09 or R30L09 spectral integrations) for the case of 1 January 1977.

c. Computational speed

The semi-implicit R30L09 A spectral model with linear ∇^4 horizontal diffusion and Manabe–Strickler radiation required 25 min per model day of cpu time on the Texas Instruments ASC computer. In comparison, the N48L09 A grid point model with conventional explicit time differencing and nonlinear diffusion required ~150 minutes of cpu time. Whether the six-fold computational advantage of the R30 model outweighs the disadvantage of having nominally coarser spacial resolution ultimately depends on the accuracy requirements. Incidentally, the length of the time step ($\Delta t \sim 20$ minutes for R30 semi-implicit versus $\Delta t \sim 3.3$ minutes for N48 conventional explicit

TABLE 1. Model characteristics for the March 1965 case and subsequent modifications.

Model characteristics	March 1965		January 1977/January 1979	
	R30L09 spectral	N48L09 grid point	R30L09 spectral	N48L09 grid point
Planetary boundary layer physics	A1 physics	A1 physics	A2 physics	A2 physics
Hydrology	Fixed $D_W = 0.5$ over land	Complete hydrologic cycle	Complete hydrologic cycle; also residual borrowing of mixing ratio replaced by local horizontal borrowing	Complete hydrologic cycle
Radiation	Manabe–Strickler	Manabe–Strickler	Manabe–Strickler	Fels–Schwarzkopf
Horizontal diffusion	Linear ∇^4 $\nu_{\nabla^4} \sim 6.4 \times 10^{15}$ m^4 s^{-1} (mean) $\nu_{\nabla^4} \sim 3.0 \times 10^{15}$ m^4 s^{-1} t < 5 days $\nu_{\nabla^4} \sim 8.0 \times 10^{15}$ m^4 s^{-1} t > 5 days	Nonlinear $k_0 = 0.25$	Linear ∇^4 $\nu_{\nabla^4} \sim 2.7 \times 10^{15}$ m^4 s^{-1} (Jan '77) $\nu_{\nabla^4} \sim 1.0 \times 10^{16}$ m^4 s^{-1} (Jan '79)	Nonlinear $k_0 = 0.25$
Time differencing	Semi-implicit leapfrog $\Delta t \sim 15$ min	Explicit leapfrog $\Delta t \sim 3.3$ min	Semi-implicit leapfrog $\Delta t \sim 20$ min	Modified economic explicit leapfrog $\Delta t \sim 5.0$ min (Jan '77) $\Delta t \sim 4.5$ min (Jan '79)
Topography	From Scripps data on 1° × 1° lat–long grid	N48 topography (slightly smoother than the R30)	From Scripps data on 1° × 1° lat–long grid	N48 topography (slightly smoother than the R30)
Virtual temperature	$T_v = T + 0.61\bar{T}q$	$T_v = \frac{T(1 + 1.61q)}{(1 + q)}$	$T_v = T$ (no virtual temperature)	$T_v = \frac{T(1 + 1.61q)}{(1 + q)}$
Vertical finite differencing	Older scheme	N48 scheme	Second order scheme	N48 scheme

time differencing) accounts for more than half of the differential in cpu time. The other factors, in order of importance, are the number of arithmetic operations intrinsic to the spectral transform versus finite difference algorithms, their vectorizability on the ASC computer and the horizontal diffusion scheme. The cpu time requirements for the N48L09 A grid point model can be reduced ~70% by using the modified economical explicit time differencing scheme.

The three case examples should provide some indication of the GFDL R30L09 A spectral model's capability at medium range forecasting. Moreover, the N48L09 results help to place the R30L09 results in perspective. However, the R30L09 versus N48L09 comparison should not be regarded as a definitive test of the *spectral* versus *finite difference* methods, in view of the inter-model differences, limited sample size and non-uniform quality of the initial conditions.

3. Initial and verification analyses

The initial analysis for 0000 GMT 1 March 1965 was synthesized from pressure level analyses of geopotential height on the northern hemispheric octagon grid by G. Cressman of the National Meteorological Center (NMC), hand analyses of tropical wind data by J. Sadler and Southern Hemispheric analyses by R. Clarke. The nonlinear balance equation was solved numerically on the modified Kurihara grid to generate an initial wind field in the extratropics. Conversely, an initial mass field was obtained in the tropics from the reverse balance equation. Proceeding with the initialization of the spectral model, the balanced wind and mass field data on constant pressure surfaces were horizontally interpolated to the relevant Gaussian latitude–longitude transform grid and vertically interpolated to 9 sigma levels. After extrapolating the geopotential height field to sea level, an initial surface pressure field was calculated, consistent with the spectral model's topography. Finally, spectral coefficients were computed for wind variables, temperature and water vapor mixing ratio at each sigma level and the logarithm of surface pressure. The initialization of the grid point model was similar but required fewer steps. The data on pressure levels were simply vertically interpolated to the 9 sigma levels, and the surface pressure

was calculated as above. Daily verification analyses were also available. But beyond 5 March 1965, they were based solely upon the NMC analysis. On those days, the mass field was extrapolated into the tropics, and balanced.

The initial conditions for 0000 GMT 1 January 1977 were derived from the GFDL 4-dimensional optimal analysis. In the GFDL analysis procedure, station data are first dynamically assimilated into the spectral model for several days prior to the initial time. This raw four-dimensional assimilation provides first guess fields for an optimum interpolation analysis. The requisite interpolations to the spectral model's grid are carried out and spectral coefficients are calculated. Also, nonlinear normal mode initialization is applied. The above analysis procedure is similar to the scheme recently described by Ploshay *et al.* (1983), although the optimum interpolation analysis step has been discarded in the latter scheme. The NMC global Hough function analyses (Flattery, 1971) were used for verification purposes. The NMC Flattery analysis is truncated at zonal wavenumber 24 and is essentially nondivergent.

The output of the forecast–analysis cycle scheme of the European Centre for Medium Range Weather Forecasts (ECMWF) was used to generate initial conditions for the case of 0000 GMT 16 January 1979. The sequence of steps in the subsequent initialization process is similar to that applied to the NMC data for 1 March 1965. However, the ECMWF pressure levels and the 1.875° resolution horizontal grid differ from NMC's, and no balancing or horizontal interfacing of data sets is required. As in the two previous cases, NMC analyses on subsequent days served as verification data.

4. Spectral versus grid point model forecast results

The medium range deterministic as well as time mean forecast capability of the GFDL R30L09 spectral model is evaluated for the 1 March 1965, 1 January 1977 and 16 January 1979 cases. For our purposes, "medium range" refers to the forecast interval between day 5 and day 15. The variables of primary interest are the geopotential height at 500 and 1000 mb, i.e., z_{500} and z_{1000}. Standard verification techniques are applied, for the most part, following Smagorinsky *et al.* (1965), Miyakoda *et al.* (1972) and others. An analysis of inter-case variability and systematic errors may be informative, even though no claim can be made for their statistical validity. The predicted medium range general circulation for the particular case of 1 January 1977 is discussed in the Appendix.

a. Deterministic forecasts

The initial z_{500} fields for the three cases are plotted in Fig. 1 on northern hemisphere stereographic maps. Those for 1 March 1965 contain the following features: A prominent ridge off the west coast of North America and downstream trough centered near the continental

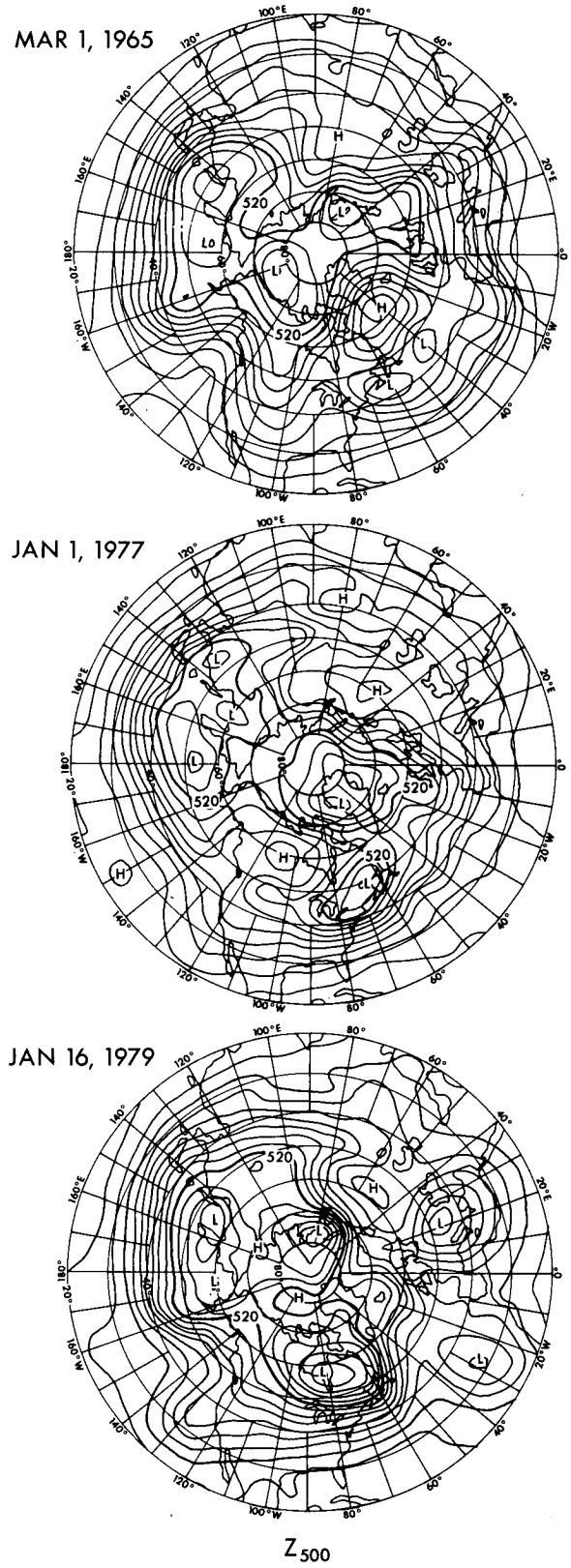

FIG. 1. Stereographic maps of the initial z_{500} fields. From top to bottom—NMC analysis for 1 March 1965, GFDL four-dimensional analysis for 1 January 1977 and ECMWF analysis for 16 January 1979. Domain is 20–90°N. Contour interval is 8 dam.

divide; and a split flow over the Atlantic consisting of an intense high pressure cell over southern Greenland and a broad trough further south.

The March 1965 forecasts of z_{500} by the GFDL R30 spectral and GFDL N48L09 grid point models are verified against observation in Fig. 2 on days 3, 4 and 10. After the initial time, the longitudinal extent of the observed split flow (Fig. 2, left hand column) increases as cutoff lows form or intensify off the southern coast of California, over the eastern United States and over the western Atlantic. The axis of the North American trough shifts to the east coast while the Greenland high weakens, propagates towards the British Isles and reintensifies.

Both forecasts are still quite good on day 3. But the R30 cutoff low over the central United States exhibits less phase lag error, and the R30 mid-Atlantic ridge has more amplitude than the corresponding N48 features. The R30 and N48 predictions share many of the same shortcomings between days 3 and 10. The

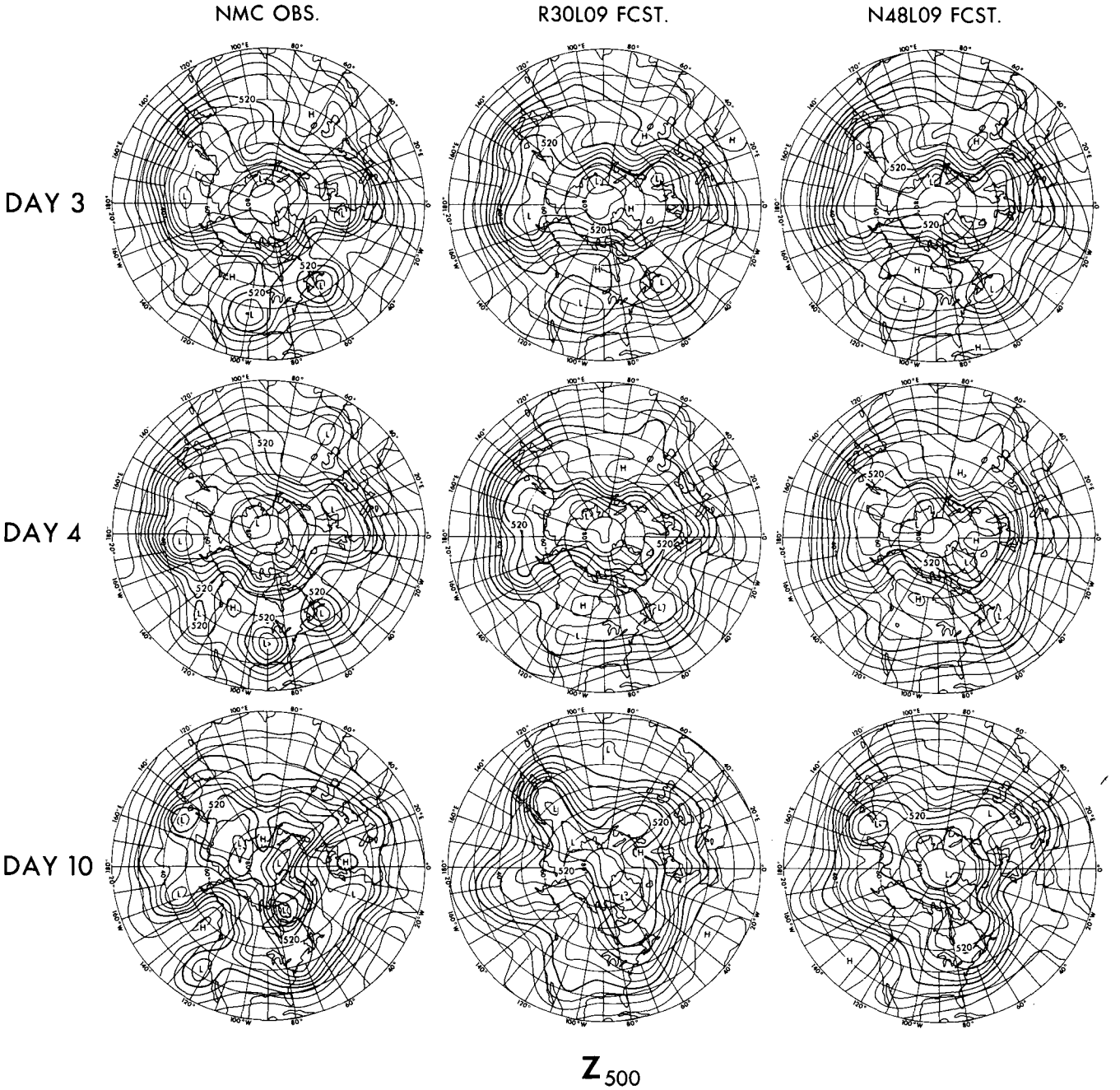

FIG. 2. Stereographic maps of z_{500} forecasts on days 3, 4 and 10 of the 1 March 1965 case. From left to right—NMC observation, R30L09 forecast and N48L09 forecast. Domain is 20–90°N. Contour interval is 8 dam.

cutoff lows over the southeastern United States and off the coast of Maine weaken dramatically by day 4. Second generation disturbances develop somewhat earlier in the grid point than in the spectral model prediction. Some residual skill still remains on day 10 at ultra-long, and possibly long wavelengths, in both forecasts. But neither is practically useful for cyclone scale disturbances beyond 4 or 5 days. The above results are consistent with the findings of Baede and Hansen (1977) for the same case. In fact, the predictions by the GFDL R30L09 and the ECMWF triangular T40L09 spectral models are quite similar.

The R30 and N48 z_{1000} forecasts (not shown) deteriorate more rapidly than the z_{500} forecasts. Residual skill is not detectable much beyond day 4.

In the 1 January 1977 case the principal observed

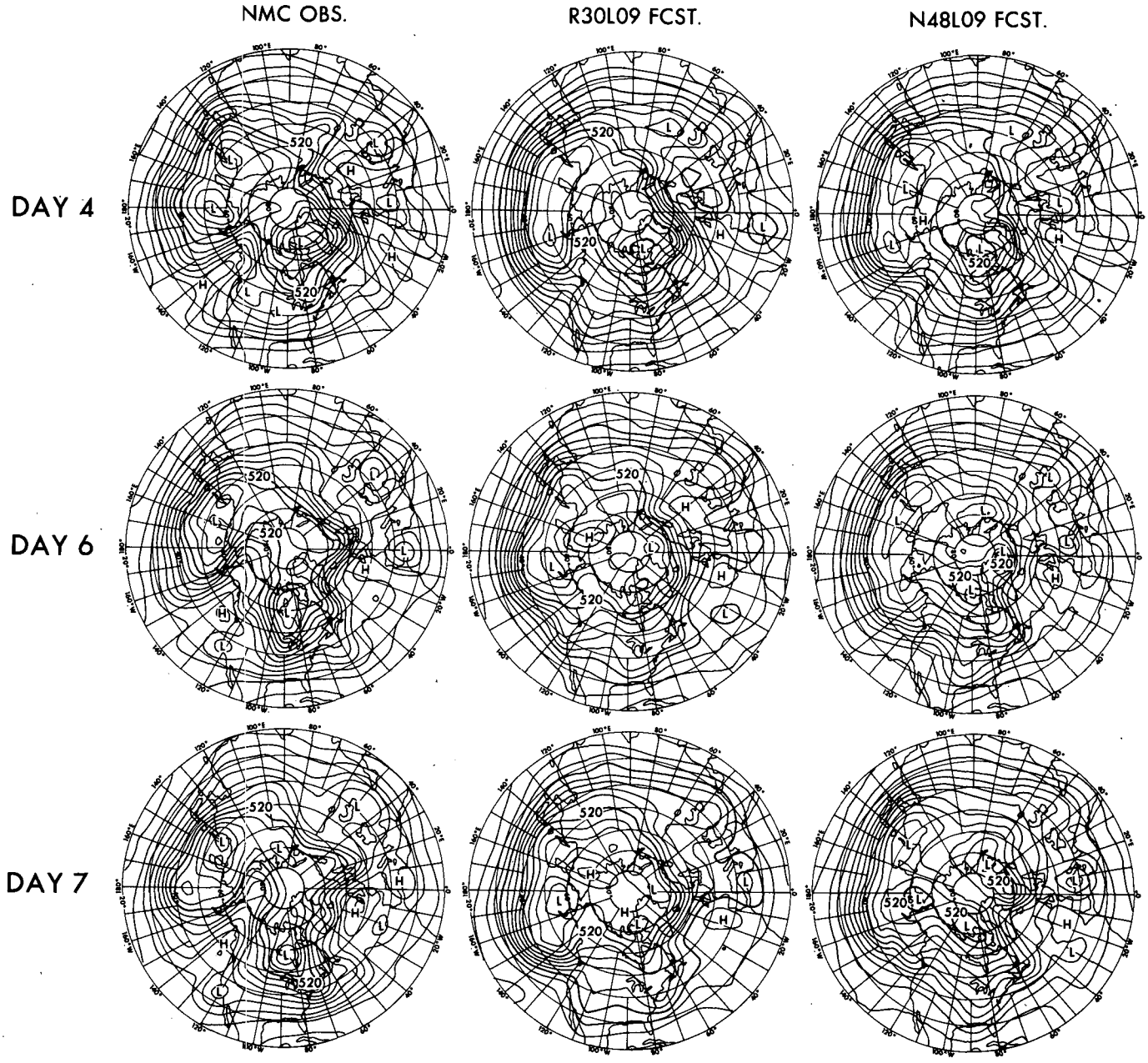

FIG. 3. Stereographic maps of z_{500} forecasts on selected days of the 1 January 1977 case between days 4 and 10. From left to right—NMC observation, R30L09 forecast and N48L09 forecast. Domain is 20–90°N. Contour interval is 8 dam.

initial features at 500 mb include intense closed vortices centered over the Canadian maritime provinces, Greenland and the north central Pacific; and split flows over Europe and over western North America. At 1000 mb (not shown) the American and Eurasian continents are both dominated by high pressure and the north-central Pacific and much of the North Atlantic by low pressure.

A sequence of spectral and grid point model z_{500} forecasts between days 4 and 10 are verified against observation in Fig. 3. The verification region is the 20–90°N latitude belt. The 500 mb observation (left hand column of Fig. 3) reveals a persistent trough over the west central Pacific. A ridge off the west coast of North America intensifies rapidly while another over northern Europe weakens. Indeed, the persistence of

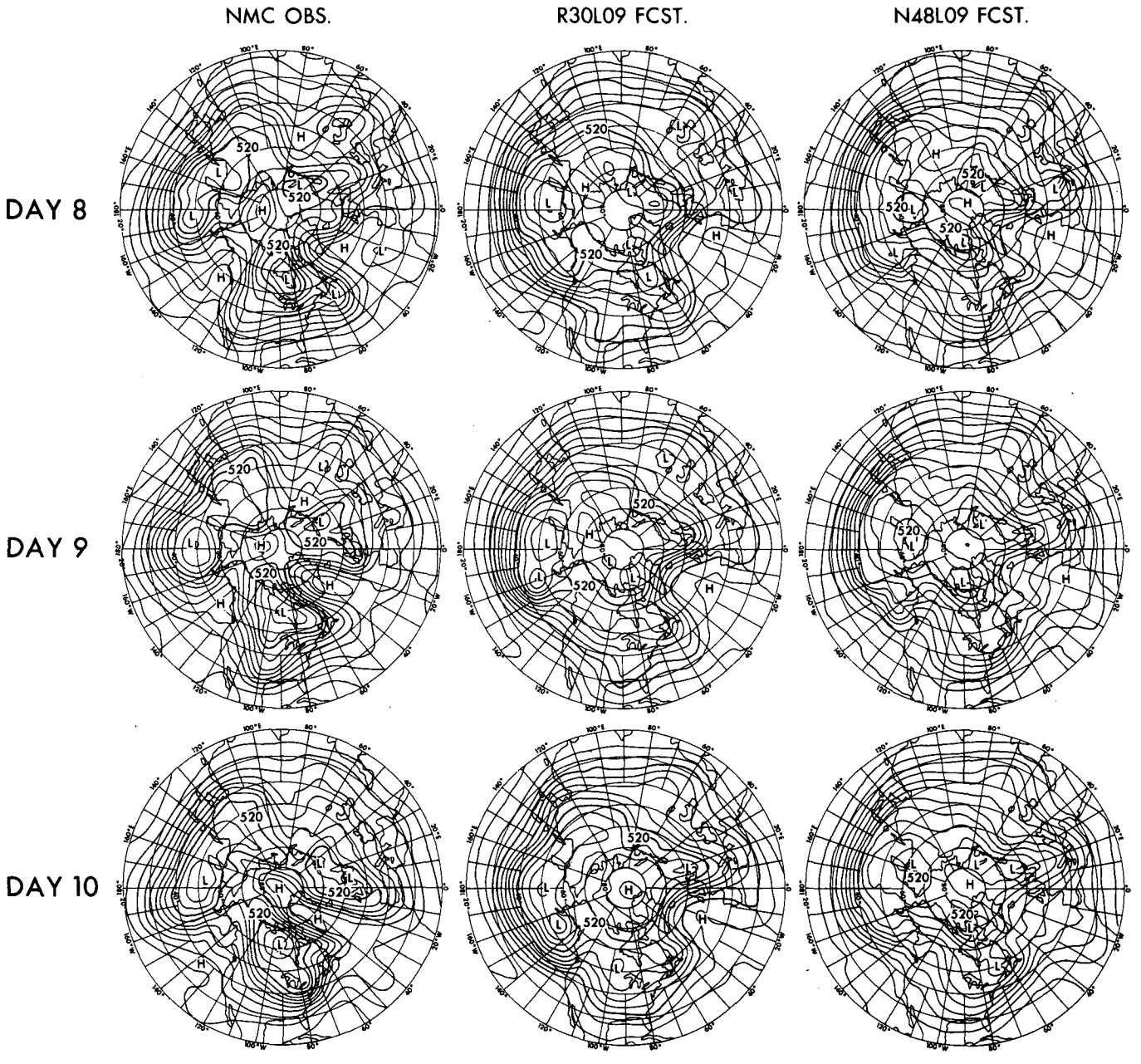

Z_{500} (continued)

FIG. 3. (*Continued*)

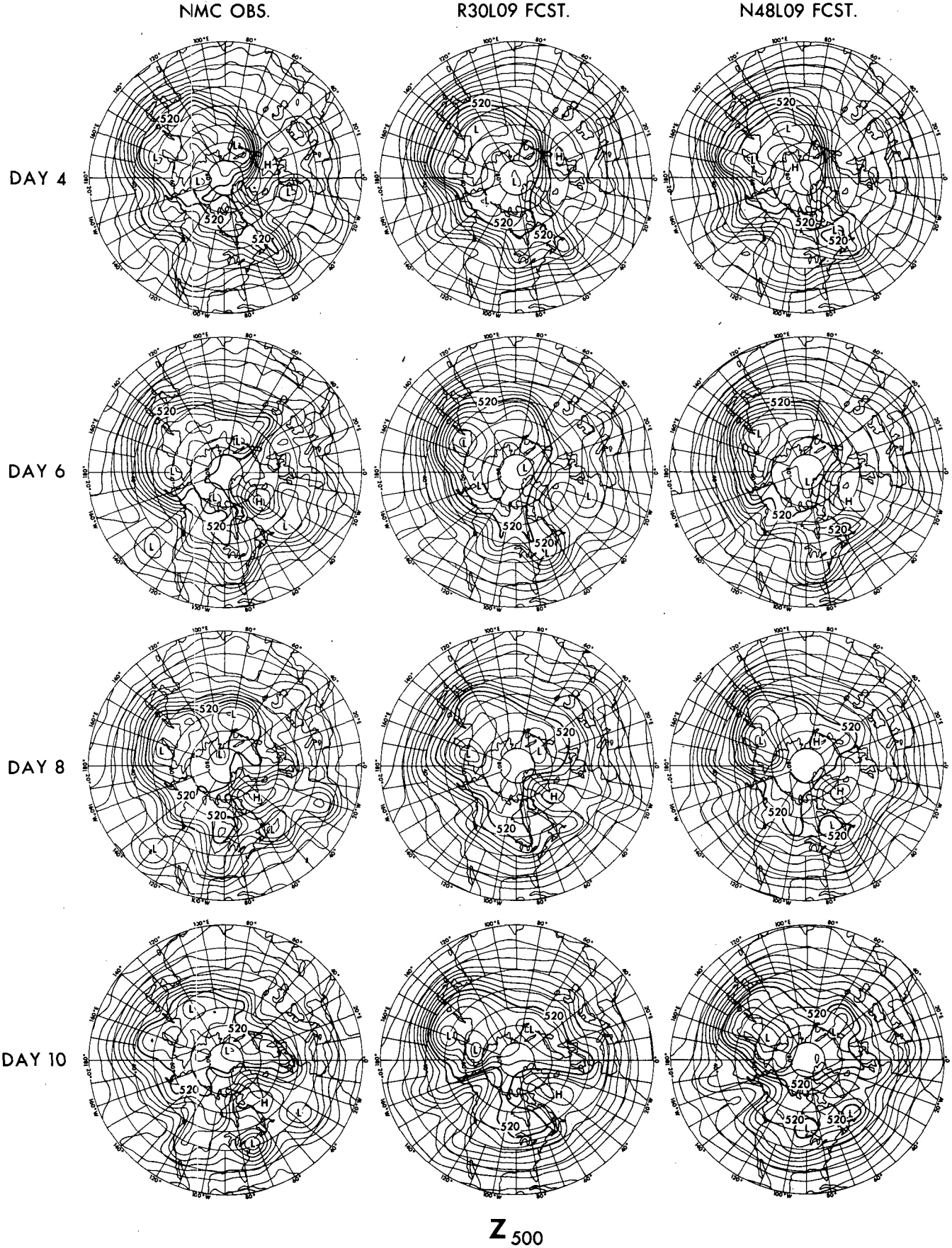

FIG. 4. As in Fig. 3 except on days 4 through 10 of the 16 January 1979 case at two-day intervals.

the intense west coast ridge and downstream North American trough are perhaps the most anomalous features of the January 1977 monthly mean circulation (Namias, 1978). Conversely, the longitudinal positions of these quasi-stationary planetary scale disturbances do not depart very much from climatology.

The spectral and grid point model predictions of z_{500} are displayed in the center and right hand columns of Fig. 3. Both predictions correspond quite well with observation for one or two days (not shown). But by day 4, the west coast ridge, among other features, is already not well-predicted by either model. The N48 and especially the R30 prediction simulate the Canadian vortex out to day 4, but fail to capture its southward thrust between day 4 and day 6. Thereafter, neither prediction adequately simulates the amplitude of the observed long wave trough over North America or upstream west coast ridge. In this respect, the R30 prediction is somewhat poorer than the N48 after day 8 or so. Conversely, the R30 quasi-stationary Atlantic ridge is more intense than the N48 on days 9–10. Also note that only the R30 prediction manages to crudely simulate the propagation of two observed transient disturbances across the United States between day 6 and day 10. The R30 transients exhibit substantial phase advance errors at first, but appear to be blocked by the R30 Atlantic ridge as they approach the east coast. On balance, the spectral and grid point model forecasts of z_{500} are of comparable quality during the first 8 or 10 days.

At 1000 mb (not shown), both predictions correspond reasonably well with observation for 1 to 2 days and qualitatively simulate many large scale features for 6 to 8 days. Individual disturbances tend to be best simulated by the R30 model between days 4 and 8 and by the N48 model on day 10.

The initial z_{500} analysis for the case of 16 January 1979 reveals an intense cutoff low over eastern Europe at 40°N, 25°E and a somewhat weaker one at 40°N, 25°W. High pressure cells are also located at 50°N, 0°E as well as at 55°N, 50°E. The stage is set for an Atlantic–European block. A time sequence of the NMC observed z_{500} field is displayed in the left hand column of Fig. 4 for the period day 4 to day 10 at 2 day intervals. As described by Bengtsson (1981), a quasi-stationary ridge over Scandinavia migrates northwest and changes its orientation. This feature in combination with troughs or cutoff lows to the southeast and southwest define a split flow over the Atlantic Ocean and Europe. After day 4, a blocking cell, centered around 60°N, 40°W becomes dominant and drifts northwest.

The evolution of the R30 and N48 z_{500} forecasts from day 4 to day 10 is displayed in the center and right hand columns of Fig. 4, respectively. As in the previous cases, the amplitude of the predicted cutoff lows and troughs becomes substantially weaker than observation. Similarly, the predicted high pressure cells over the Atlantic do not attain the observed amplitude. Nonetheless, the R30 and N48 models predict the phase and maintenance of the Atlantic block surprisingly well. On day 10 the observed split flow, European trough and Atlantic ridge are predicted somewhat more accurately by the R30 model. On day 15 (not shown), all of these features have disappeared in the N48 prediction, whereas the R30 still simulates the trough and ridge. Note that the R30 model successfully maintains the ridge off the west coast of North America, which is located 30°W of the January 1977 ridge. As in the 1 January 1977 case, the R30 transients over North America propagate too rapidly at first, but are retarded by the Atlantic block as they approach the east coast.

The R30 and N48 forecasts of z_{1000} (not shown) are also very good. For approximately 6 days, the predicted versus observed cyclone and larger scale features exhibit a one-to-one correspondence. Thereafter, the R30 and N48 models qualitatively simulate the block out to 15 days and 12 days, respectively. However, the predicted lows over the Atlantic are too weak and substantial phase errors occur over North America, as at 500 mb.

The quality of the initial data was presumably very good for the 16 January 1979 case, since it coincides with the first special observing period of the First GARP Global Experiment (FGGE). High quality initial data might be especially beneficial for relatively predictable patterns.

Hovmöller trough–ridge diagrams can provide useful supplementary verification of the geopotential height forecasts. Diagrams of the total predicted and observed z_{500} fields, averaged over the 40–50°N midlatitude belt (Fig. 5), reveal quasi-stationary planetary scale features as well as transient disturbances. The Fourier wavenumber 6–10 band contribution to z_{500} (Fig. 6) is traditionally associated with localized, cyclone scale transient disturbances, although the latter project onto a considerably broader Fourier spectrum (Williamson, 1981).

The correspondence between predicted and observed features is somewhat case-dependent. But it tends to last at least 3 or 4 days for cyclone scale transient disturbances and beyond 10 days for planetary scale disturbances. In the 1 March 1965 case (not shown), the R30 prediction of z_{500} is slightly inferior to the N48 after day 5. In particular, the R30 ridge near the west coast of North America is substantially weaker than its N48 or observed counterparts and exhibits erroneous eastward propagation. But not all of the R30 planetary scale disturbances (e.g., the downstream North American trough) are weaker than the N48.

In the 1 January 1977 case (Fig. 5a), neither model builds a quasi-stationary west coast ridge, contrary to observation, between day 2 and day 5. Yet, intriguingly, the grid point model does build and maintain one after day 5. In comparison, the spectral model builds a considerably weaker ridge after day 5 and has difficulty maintaining it. This deficiency contributes to the zonal

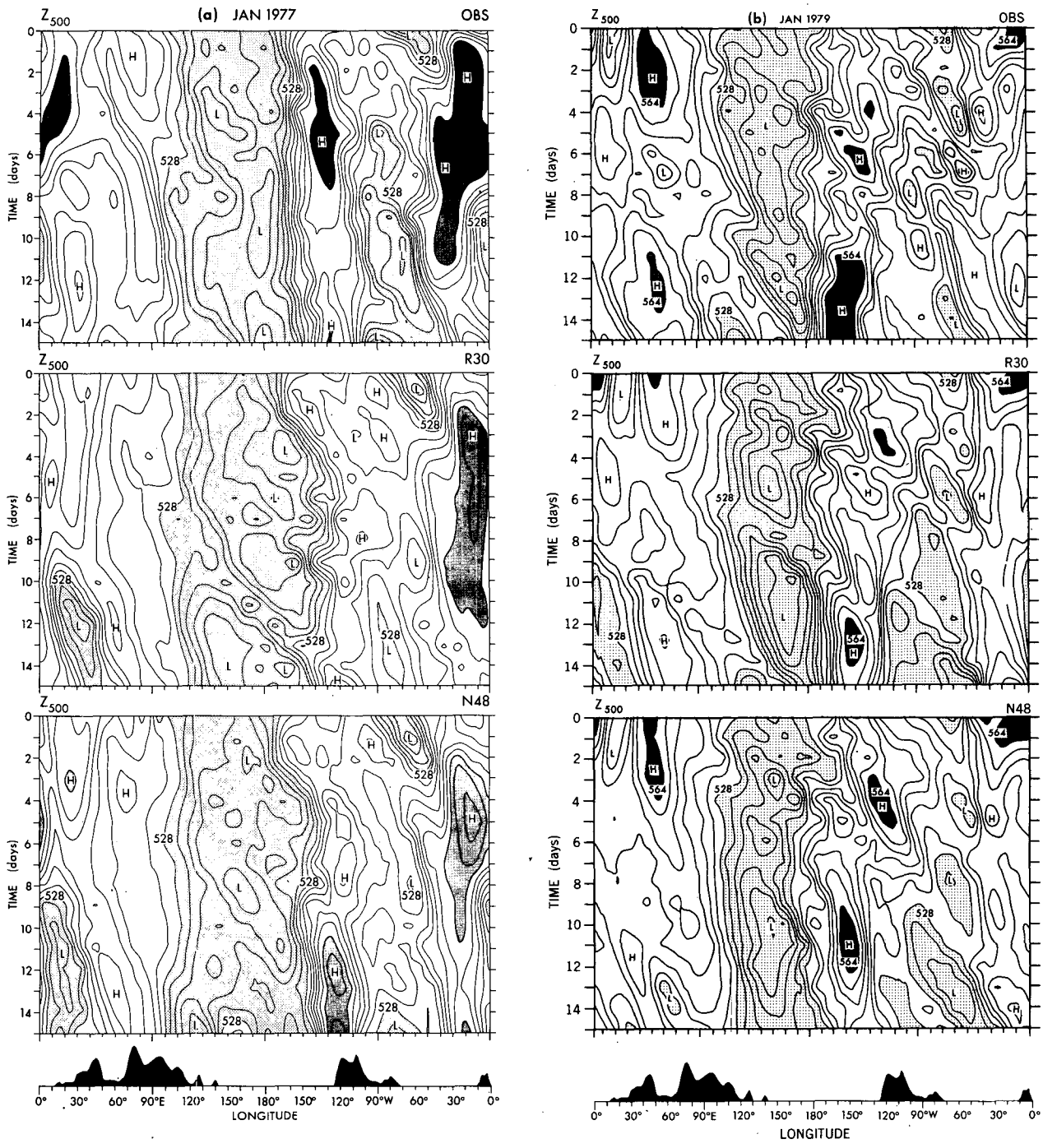

FIG. 5. Hovmöller trough–ridge diagrams of the observed (top) R30L09 (center) and N48L09 (bottom) z_{500} fields from day 0 to day 15 for (a) 1 January 1977 case and (b) 16 January 1979 case. Domain is 40–50°N. Contour interval is 6 dam. $z \leq 528$ dam where sparsely shaded, $z \geq 564$ dam where densely shaded. The terrain is indicated schematically.

bias. A plausible scenario is as follows. A succession of intense R30 transient depressions propagates eastward from the quasi-stationary Pacific trough. They propagate more rapidly than their N48 or observed counterparts. Thus they have less opportunity to be damped prior to reaching the vicinity of the downstream west coast ridge. This situation is aggravated further by the R30 model's weak and highly scale selective ∇^4 horizontal diffusion. Consequently, the ridge may be temporarily flattened by each passing R30

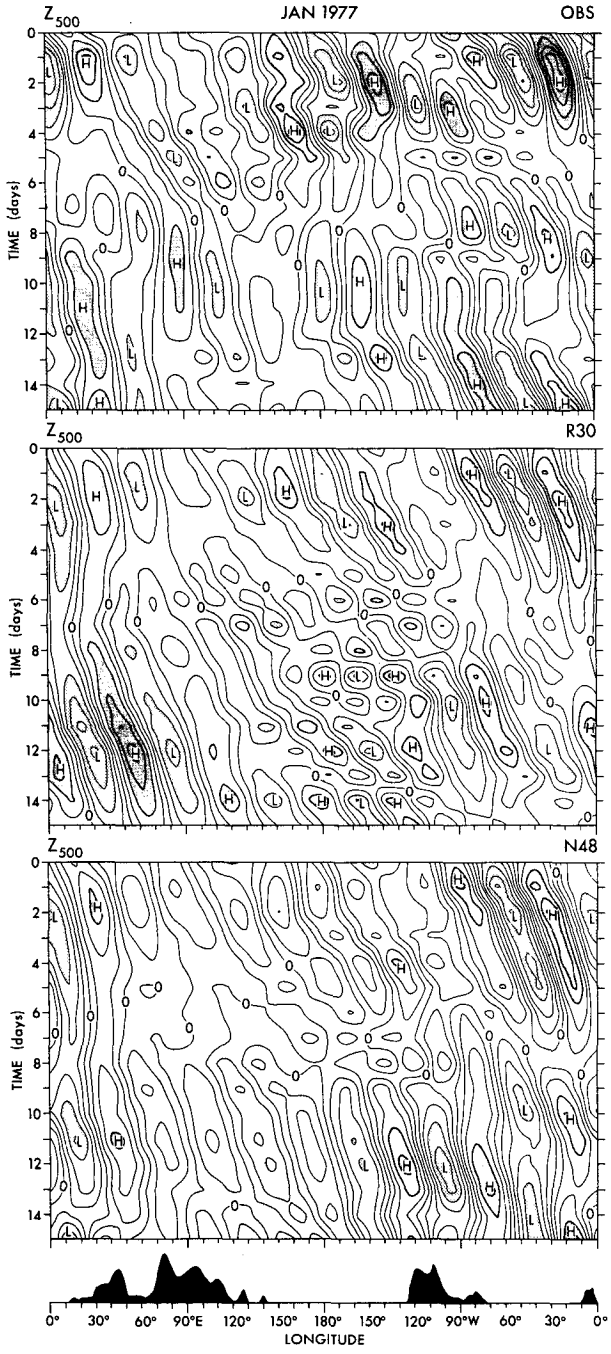

FIG. 6. As in Fig. 5a, except that the contribution of only wavenumbers 6 to 10 is displayed. Also, the contour interval is 3 dam and heights are $\leqslant -6$ dam or $\geqslant +6$ dam in sparsely and densely shaded regions, respectively.

transient cyclonic disturbance. The intensity of the R30-predicted transients is suggested by the wavy contours between the R30 Pacific trough and downstream ridge (Fig. 5a) beyond day 6. Similarly, their rapid propagation over the central and eastern Pacific ocean is apparent in the Hovmöller diagram for the wavenumber 6–10 band (Fig. 6) after day 4. It is consistent with the strongly zonal R30 flow over the eastern Pacific (J. D. Mahlman, personal communication, 1982), whereas the N48 and observed flows have a significant meridional component near the west coast of North America. As for indirect evidence of underdamping, the R30 transients in the wavenumber 6–10 band are substantially noisier than their N48 counterparts.

The midlatitude transients may also be affected to some extent by excessive amplitude inertia–gravity oscillations in the tropics. The R30 surface pressure record in the tropics (not shown) was permeated by local oscillations of as much as 8–10 mb during the first 12 h of integration. Their excitation and slow decay were presumably related to a combination of poor initialization, shocking viz. convective adjustment, sluggish geostrophic adjustment and insufficient damping. According to observing systems simulation experiments by Gordon *et al.* (1972), the tropics can affect the midlatitudes within 7–10 days. Also, Somerville (1980) has shown that unrealistic initial conditions in the tropics can influence ultralong waves at midlatitudes even sooner.

Another prominent feature of Fig. 5a is the North American trough. Both models, especially the spectral, underpredict its amplitude. As for the Atlantic ridge, neither model retrogrades it enough and only the R30 model maintains the observed amplitude after day 7. The R30 and N48 trough and ridge over Europe are situated too far east on day 10 and continue to propagate eastward between day 10 and day 15.

In summary, the N48 z_{500} forecast from 1 January 1977 initial conditions deserves a slightly higher rating than the R30 between day 5 and day 10, based upon Figs. 5a and 6. The grid point models' superiority is more clear cut in the 10–15 day range.

Hovmöller diagrams of z_{500} for the 16 January 1979 case are illustrated in Fig. 5b. Beyond day 5, the predictions simulate the observed propagation of transients better than in the previous two cases. Likewise, the simulations of the observed quasi-stationary features are good. The Hovmöller diagrams do not indicate an intense Atlantic blocking ridge, however, because the predicted or observed ridges are centered well north of the 40–50°N latitude domain. For related reasons, there is only a slight hint that the R30 prediction of the Atlantic ridge is better than the N48 after day 10. These results indicate that Hovmöller diagrams need to be interpreted cautiously.

The predictions of geopotential height have also been verified objectively. A standard technique used by Miyakoda *et al.* (1972) is the anomaly correlation, i.e., the correlation between the departures of a forecast and observation from climatology. In the 1 March 1965 case the time mean observation for 6–16 March 1965 actually served as the March climatology. The anomaly correlation is evaluated for the 29–90°N latitude domain.

The R30 anomaly correlations coefficients $r(z_{500})$ of z_{500} corresponding to all three cases are plotted versus time in Fig. 7. Also, the R30 versus N48 results for $r(z_{500})$ and $r(z_{1000})$ are compared case by case in Figs. 8 and 9, respectively. Clearly, $r(z_{500})$ is very case-dependent. For the best case, i.e., 16 January 1979, the period of practically useful skill of the spectral model forecast exceeds 11 days at 500 mb, according to the $r \geq 0.6$ criterion of Jarraud *et al.* (1981). In fact, judging from Table 4 of Bengtsson (1981), the R30 model may have performed slightly better than the finer resolution ECMWF P63L15 model. (Here P denotes a pentagonal shaped spectral domain). But for the other two cases, the period of practically useful skill at 500 mb is only 3.5 and 4.5 days. A comparison of Figs. 7 and 8 indicates that $r(z_{500})$ tends to be less model-dependent than case-dependent during the first 10 days. Furthermore, the relative ranking of the R30 and N48 results is case-dependent. For example, whereas the N48 model verifies better in the case of 1 January 1977, the spectral model verifies better in the case of 16 January 1979. Both model forecasts of z_{500} consistently exhibit higher correlations than persistence, out to 10 days. At 1000 mb (Fig. 9), the period of practically useful skill is greater for either January case than for the March 1965 case.

b. Time mean forecasts

The R30 and N48 time mean forecasts of z_{500} and z_{1000} are verified against observation in Figs. 10 and 11, respectively. The format of these figures permits cross-case comparisons as well as model intercom-

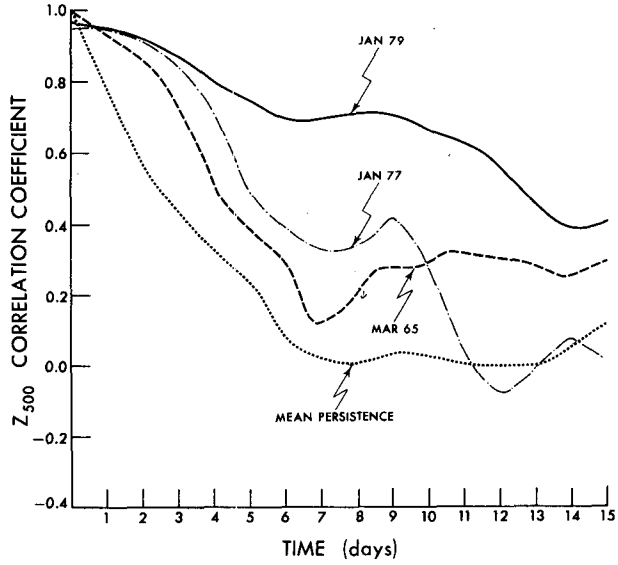

FIG. 7. Anomaly correlation of R30L09 vs observed z_{500} fields for the 1 March 1965, 1 January 1977 and 16 January 1979 cases. The ensemble mean of the persistence curves for the individual cases is also plotted. Domain is 29–90°N.

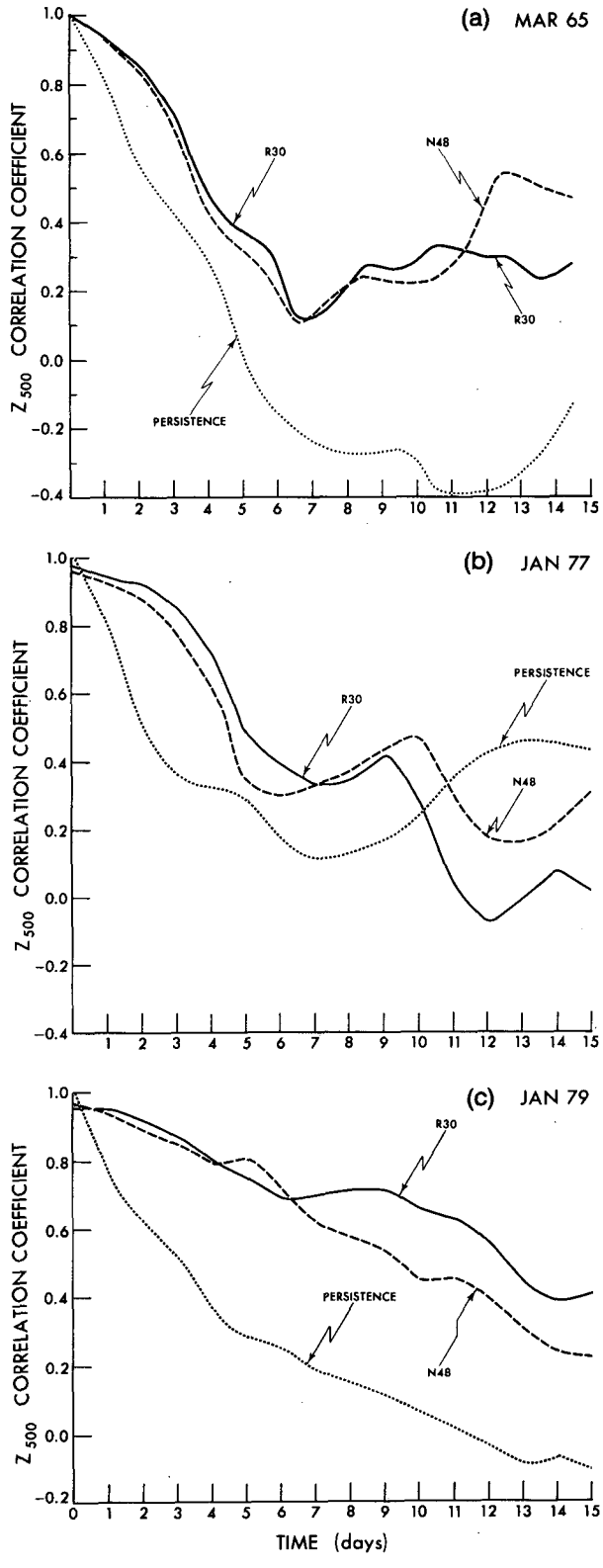

FIG. 8. Anomaly correlation of R30L09 vs observed, N48L09 vs observed, and persistence vs observed z_{500} fields for (a) the 1 March 1965 case, (b) the 1 January 1977 case and (c) the 16 January 1979 case. Domain is 29–90°N.

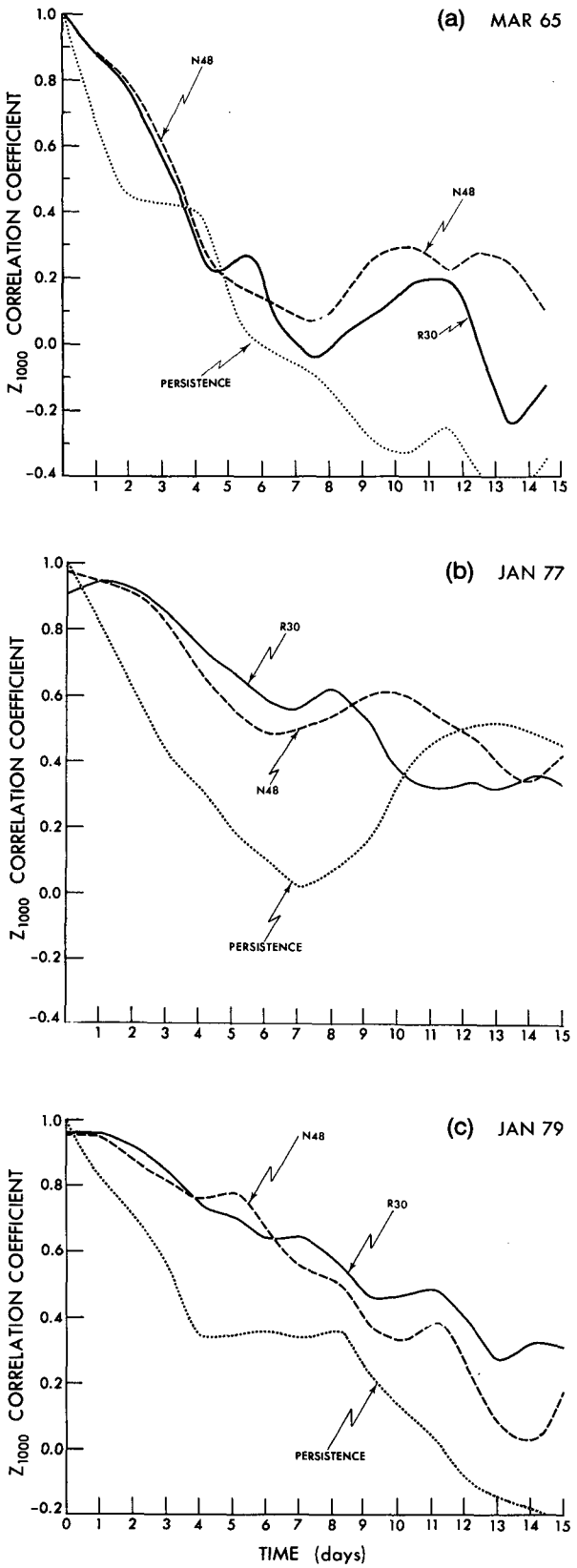

FIG. 9. As in Fig. 8 except that z_{1000} fields are correlated.

parisons for a particular case. The time interval used for averaging is day 5.5–14.5 in the 1 March 1965 case and day 5–15 in the two January cases. Thus, the influence of the short range forecast is excluded and the variance due to cyclone scale transient disturbances is significantly reduced.

In the 1 March 1965 case, both models handle the time mean prediction of the major planetary scale waves at 500 mb quite well. The spectral model predicts the phase of the ridge over western North America and the troughs over the eastern seaboard more accurately than the grid point model and gives a hint of the split flow over Europe. On the other hand, the amplitude of the R30 ridge over western North America and trough off the southern California coast are too weak. The grid point model develops the latter trough more realistically.

In the 1 January 1977 case (Fig. 10 middle row), the phases of the predicted quasi-stationary planetary waves at 500 mb correspond qualitatively with observation. But on closer inspection, the predicted time mean position of the west coast ridge is inland, whereas, the observed position is just off the west coast of North America. The R30 ridge is furthest inland. Perhaps the most notable shortcomings of both forecasts are that the predicted amplitudes of the quasi-stationary planetary waves are too weak and the subpolar Canadian vortex has not plunged southward. Note that the R30 amplitudes are significantly weaker than the N48 (and weaker than in the other two cases). For this reason the N48 simulation at 500 mb is judged to be better, overall, than the R30. Although our model has not yet converged to its quasi-equilibrium climatology, it is interesting that an underdamped GCM can generate excessively symmetric westerly jets. The latter finding was obtained by Dr. J. D. Mahlman (personal communication, 1982).

In January 1977, the correspondence between predicted and observed quasi-stationary features is worse at 1000 mb (Fig. 11, middle row) than at 500 mb. Whereas both models simulate the Siberian high quite well, the predicted flows over the North Central Pacific extend too far eastward. The N48 Pacific low is roughly 100 m weaker than observed whereas the R30 is nearly 90 m too intense. Over the Atlantic Ocean–western European sector, the N48 predicted disturbances are perhaps somewhat more realistic overall, than the R30.

The most accurate time mean predictions of z_{500} and z_{1000} are achieved in the 16 January 1979 case (see Fig. 10, bottom row and Fig. 11, bottom row, respectively). Furthermore, the R30 prediction is superior, overall, to the N48. In particular, at 500 mb, the R30 prediction best simulates the strength of the trough over Europe, the phase of the Atlantic and Aleutian ridges, the shape of the trough over North America and intensity of the ridging off the west coast of the United States. Of course, there are some substantial discrepancies as well. For example, the models

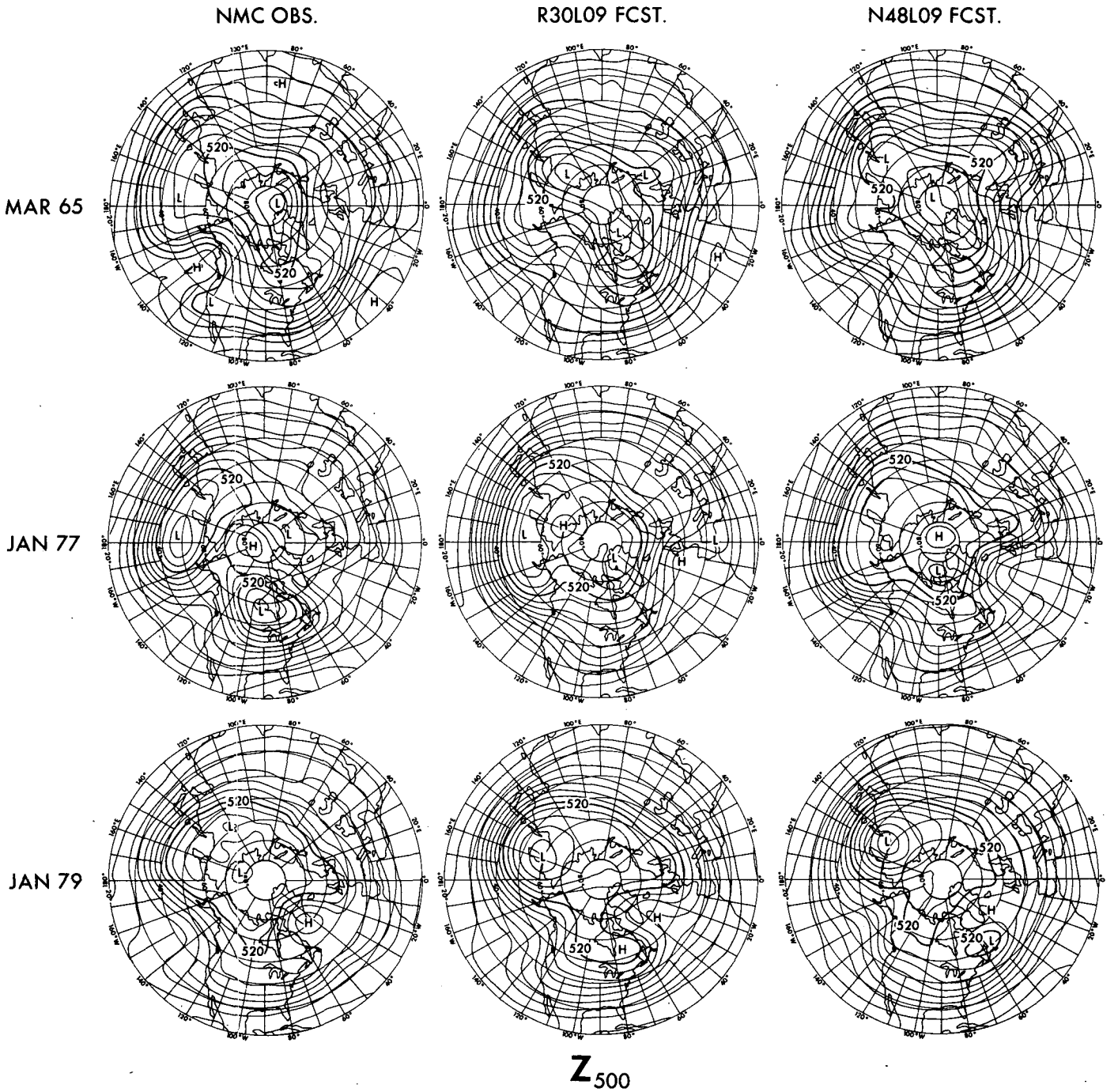

FIG. 10. Stereographic maps of day 5–15 time-averaged z_{500} fields. From left to right—observation, R30L09 forecast and N48L09 forecast. From top to bottom—1 March 1965 case, 1 January 1977 case and 16 January 1979 case. Domain is 20–90°N. Contour interval is 8 dam.

do not reproduce the troughlike character of the southern branch of the Atlantic block and they overdevelop the trough over Siberia and ridging over the Aleutians.

As at 500 mb, the major features of the predicted geopotential height field at 1000 mb correspond one-to-one to observation. The main discrepancies relate to the latitudinal position of the observed Newfoundland low (R30 and N48); phase and intensity of the observed North Sea low (R30); separation of the Newfoundland and North Sea lows (N48); the phase (N48) and orientation and size (R30 and N48) of the Bering Sea low.

In the remainder of of this section, ensemble mean error fields (at 500 mb) and longitudinal–height cross

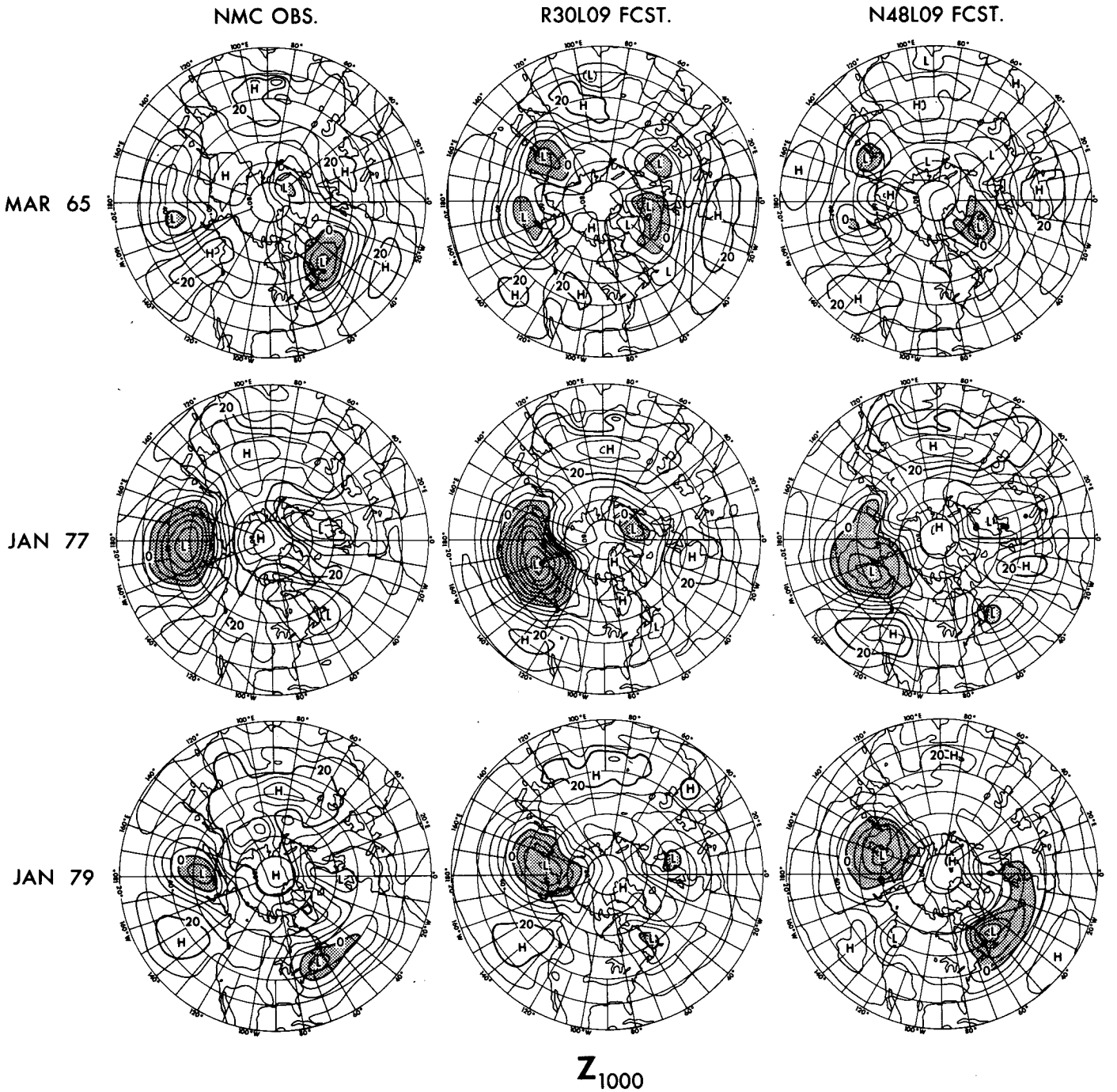

FIG. 11. As in Fig. 10 except for z_{1000}. Also, contour interval is 4 dam and $z \leq 0$ dam in stippled regions.

sections (at latitude 45°N) are presented for the R30 and N48 time mean geopotential height field. The ensemble means conveniently provide information about the mean biases for the three particular cases investigated. However, due to the small sample size, the ensemble means are not necessarily representative of the results obtainable from a much larger sample.

Ensemble mean R30 and N48 z_{500} error fields have been computed in a straightforward manner from the individual day 5–15 time mean error fields for the three cases. The results are mapped in Fig. 12, along with the ensemble mean "observed" transient variability (OTV). To compute the OTV of z_{500} for a particular case, the appropriate day 5–15 time mean value

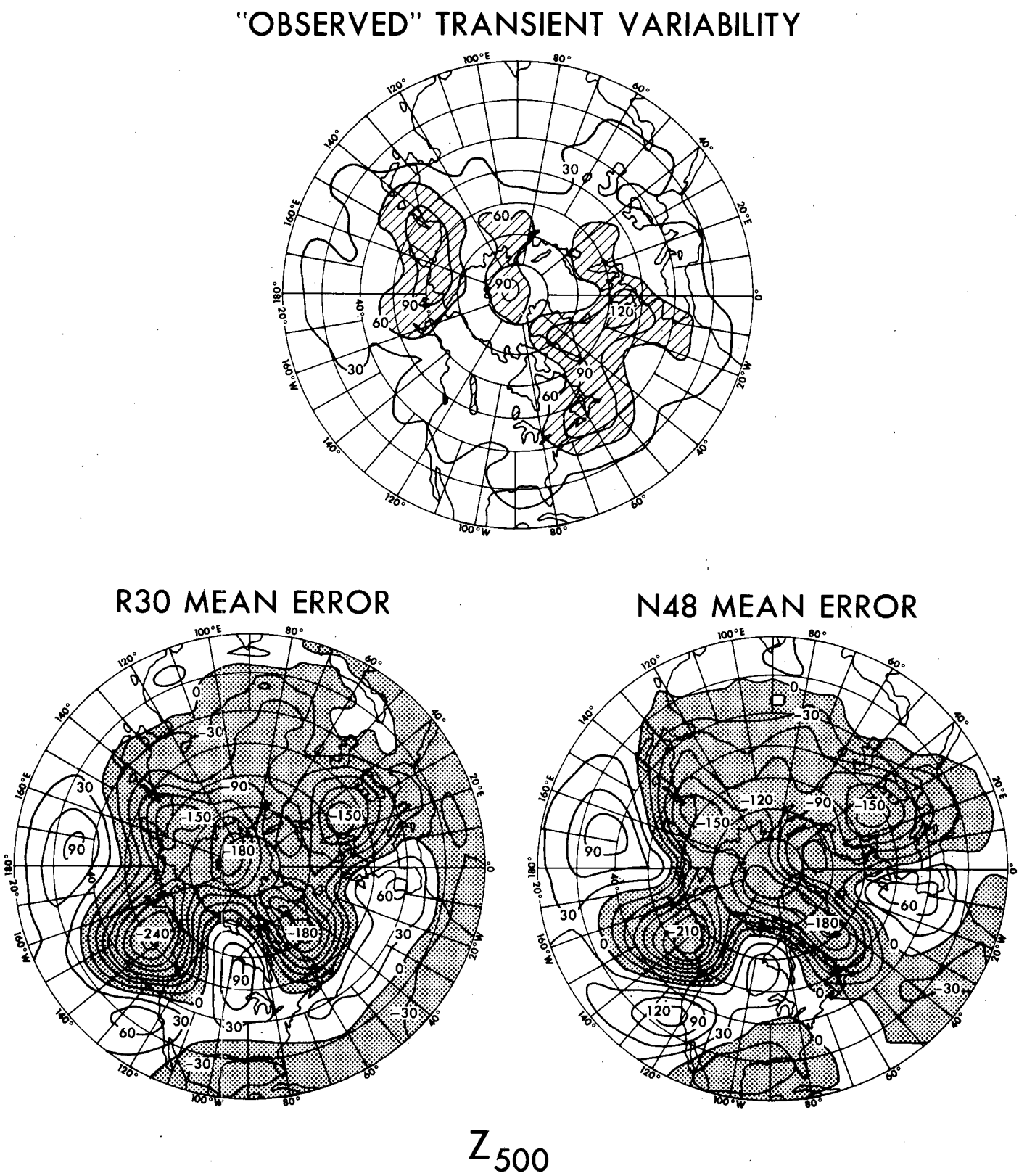

FIG. 12. Stereographic maps of three-case ensemble mean observed transient variability (OTV) of z_{500} (top) and R30L09 and N48L09 time mean forecast error of z_{500} (bottom). Time averaging period ~ day 5 to day 15. Domain is 20–90°N. Contour interval is 3 dam. OTV > 6 dam in hatched regions. Forecast error < 0 in stippled regions.

is first subtracted from the observed daily value. Then the OTV is the root mean square of the daily residuals over the day 5–15 period.

The R30 and N48 predictions have qualitatively similar systematic biases. However, the underdevelopment of the observed ridge off the west coast of North America (excluding southern California) and the downstream North American trough are more pronounced in the R30 predictions. Note that the apparent model biases in those regions would be accentuated even more if normalized by the local OTV field.

The ensemble mean longitude–height cross sections of R30 and N48-predicted as well as observed geopotential height at 45°N are illustrated in Fig. 13. The predicted long waves tend to tilt westward with height, in qualitative agreement with observation. However, the R30 and N48 Pacific–North American ridges are underdeveloped, especially in the upper troposphere. Also, the predicted troughs immediately downstream do not extend far enough east and lack a clear-cut minimum near the surface. Farther downstream, the predicted ridging over the northeast Atlantic is exaggerated, consistent with the positive bias in Fig. 12. Meanwhile, the R30 and N48-predicted amplitudes of the Pacific trough are quite realistic although the predicted centers, especially the N48, are located too far west.

5. Diffusion sensitivity experiments

Earlier, we suggested that the R30L09 spectral model solution may be underdamped, particularly for the case of 1 January 1977, when $\nu_{\nabla^4} = 2.68 \times 10^{15}$ m^4 s^{-1}. As a follow-up, comparative integrations were carried out for this case using four versions of the R30L09 global spectral model: (i) "A2"—conventional "A2" physics including ∇^4 horizontal diffusion with $\nu_{\nabla^4} = 2.68 \times 10^{15}$ m^4 s^{-1}; (ii) "A2+"—the same as "A2" except that $\nu_{\nabla^4} = 1.0 \times 10^{16}$ m^4 s^{-1}, i.e., nearly 4 times stronger; (iii) "A2-NLV"—the same as "A2" except for nonlinear horizontal diffusion with $k_0 = 0.20$; (iv) "E4-NLV"—the "E4" physics plus nonlinear horizontal diffusion with $k_0 = 0.20$.

In the "NLV" models, the nonlinear diffusion is proportional to k_0^2 (see Eqs. (49)–(52), (56a) and (56b) of GS). For reference, $k_0 = 0.25$ in the N48L09 "A2"

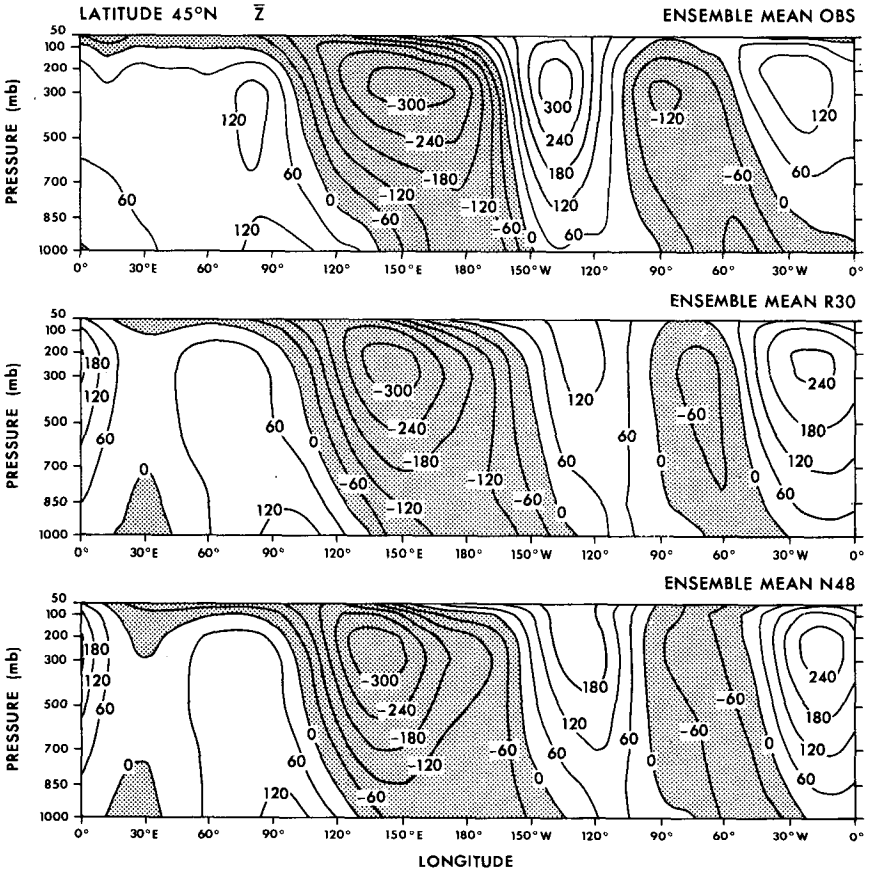

FIG. 13. Longitude–height cross sections of the ensemble mean, day 5–15 time mean z_{500} fields, with zonal mean removed, at 45°N. NMC observation (top), R30L09 forecast (center) and N48L09 forecast (bottom). Contour interval is 6 dam. $z < 0$ in stippled regions.

model. Meanwhile, in all of the "A2" models, Prandtl vertical mixing is applied to the wind and water vapor fields but not to the temperature field. The Prandtl mixing length is assumed to decrease linearly from 30 m at sigma level 9 to 0 at level $5\frac{1}{2}$. The A2 thermal vertical mixing is accomplished viz. dry convective adjustment. Three distinguishing features of "E4" physics are the Monin–Obukhov surface boundary layer formulation, the Mellor and Yamada (1974) turbulent closure scheme in the planetary boundary layer and free atmosphere, and suppression of dry convective adjustment.

All integrations were started from the GFDL 1 January 1977 initial conditions. The day 5–15 time mean predictions of z_{500} are shown in Fig. 14. The sensitivity of the amplitude of quasi-stationary planetary waves to diffusion is of primary interest. The west coast ridge, downstream North American trough, Atlantic ridge and downstream European trough amplify considerably when "E4" physics is specified. Also, stronger ∇^4 horizontal diffusion produces noticeable amplification of the latter two features. In comparison, nonlinear horizontal diffusion alone ($k_0 = 0.20$) has little effect on the day 5–15 time mean solution. Between day 10 and 20, the phase propagation of the "E4-NLV" transients (not shown) retains some correspondence with observation. Presumably, the transients are being advected by a somewhat realistic larger scale flow field.

The corresponding R30L09 "A2", "A2+", "A2-NLV" and "E4-NLV" monthly mean predictions of z_{500} are illustrated in Fig. 15. The intensity of the "E4-NLV" planetary waves clearly stands out in Fig. 15, although even the "E4-NLV" flow becomes more zonally symmetric after day 20. Strictly speaking, in all four monthly mean predictions, the planetary wavenumber 1 mode contains considerable variance. However, this variance is mainly associated with longitudinal variations in the intensity, but not in the meandering of the predicted jets. Thus, improved diffusion appears to delay but not prevent the partial decay of the predicted quasi-stationary meandering planetary waves, at least in the 1 January 1977 case.

In hindsight, the value of the nonlinear horizontal diffusion parameter k_0, i.e., 0.20 was probably too

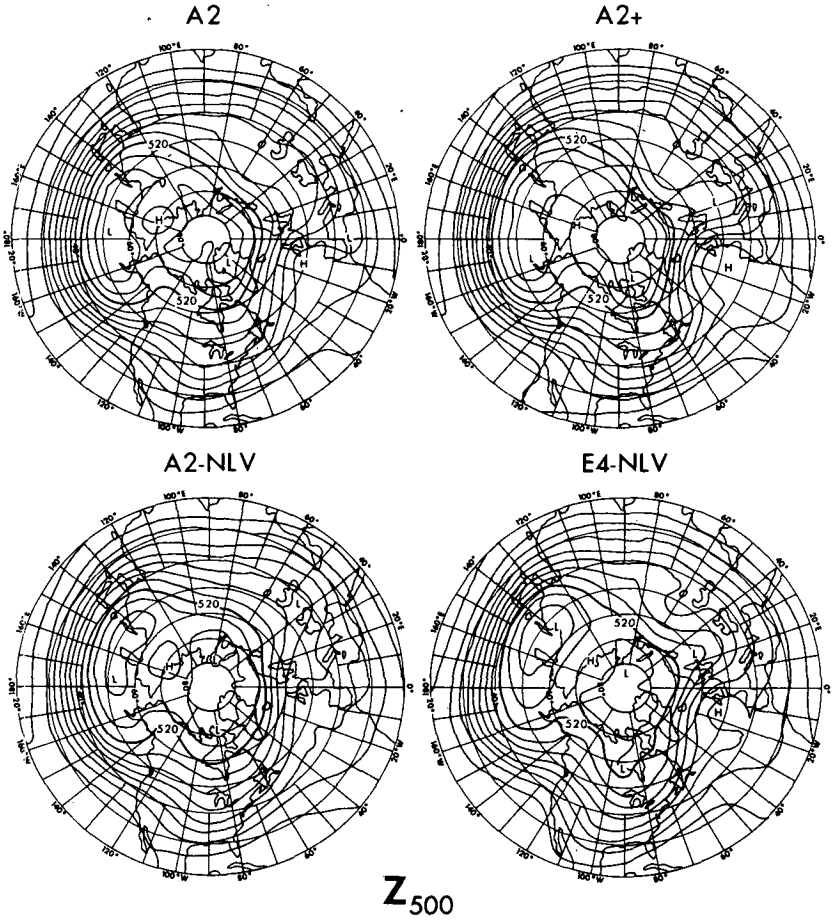

FIG. 14. Stereographic maps of the day 5–15 time mean forecasts of z_{500} for the 1 January 1977 case. R30A2 (upper left) R30A2-NLV (lower left), R30A2+ (upper right) and R30E4-NLV (lower right). Domain is 20–90°N. Contour interval is 8 dam.

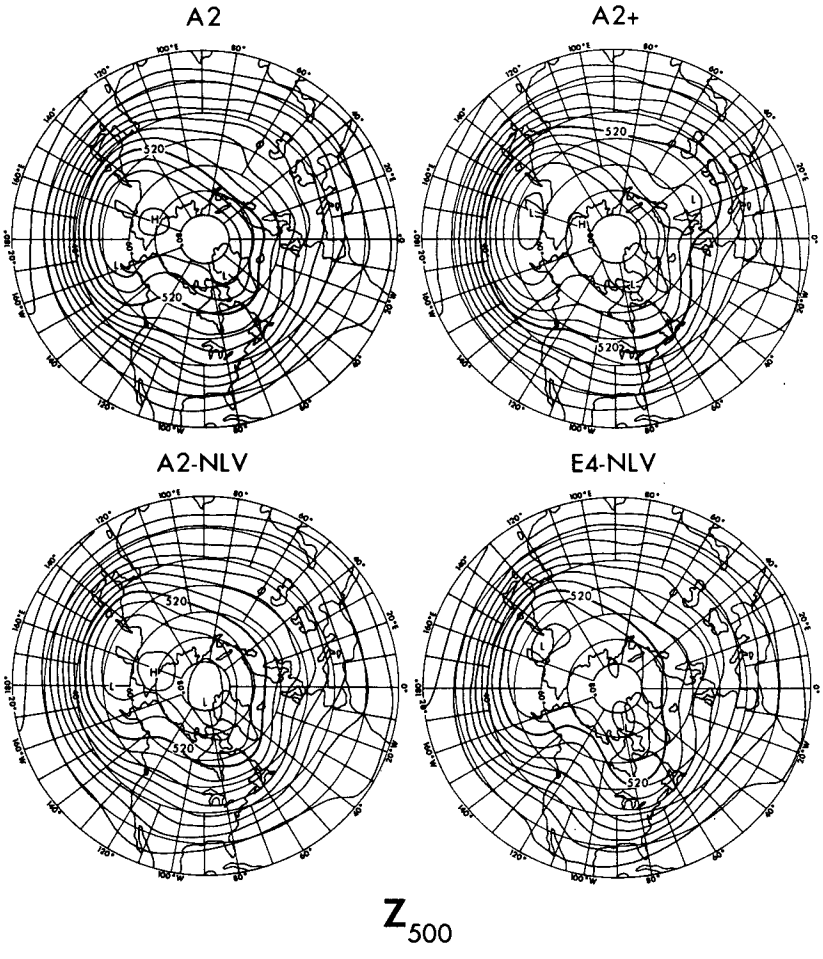

FIG. 15. As in Fig. 14 except for monthly mean forecasts of z_{500}.

weak. Also, the linear ∇^4 horizontal diffusion did not effectively damp disturbances of intermediate length scale, judging from the e-folding damping time τ_d

$$\tau_d(n) = \frac{a^4}{\nu_{\nabla^4}[n(n+1)]^2}, \quad (1)$$

where a is the earth's radius and n is the two dimensional wavenumber corresponding to the lower subscript of the associated Legendre polynomial P_n^m. Setting $n = 20$ and $\nu_{\nabla^4} = 2.68 \times 10^{15}$ m^4 s^{-1}, $\tau_d(20) \sim 40$ days.

The January 1977 day 6–15 time mean, latitude mean Fourier kinetic energy spectra

$$E_m = [(2 - \delta_{m,0})|E_{(m)}|^2/2]^{-\varphi,t} \quad (2)$$

and Fourier enstrophy spectra

$$\epsilon_m = [(2 - \delta_{m,0})|\zeta_{(m)}|^2/2]^{-\varphi,t} \quad (3)$$

at 500 mb are germane to the present discussion. In Eqs. (2) and (3), $E_{(m)}$ and $\zeta_{(m)}$ are Fourier coefficients corresponding to the spectral kinetic energy E and relative vorticity ζ, m is the zonal wavenumber, $\delta_{m,0}$ the Kronecker delta function and $(-\varphi, t)$ denotes the application of latitude–time averaging. The R30, N48 and observed spectra were calculated in a self-consistent manner. The wavenumber range $0 \leqslant m \leqslant 42$ was chosen to adequately resolve the N48 enstrophy spectrum. A negligible amount of R30-predicted enstrophy leaked into wavenumbers $m > 30$, due to the vertical interpolation of the horizontal wind field from sigma to pressure surfaces. The originial NMC Flattery analyses were truncated at zonal wavenumber $m = 24$. However, as part of our own initialization procedure, the temperature field was dry convectively adjusted in vertical columns. The subsequent spectral truncation of the adjusted fields redistributed some thermal variance into higher modes, i.e., corresponding to $m \geqslant 25$. Likewise, the vertical diffusion terms were affected by spectral truncation, but only weakly.

Bar graphs of the day 6–15 time mean R30A2, R30A2+, R30E4-NLV, N48 and observed kinetic energy spectra at 500 mb and 34–55°N extratropics belt are displayed in Fig. 16, where the focus is on the low

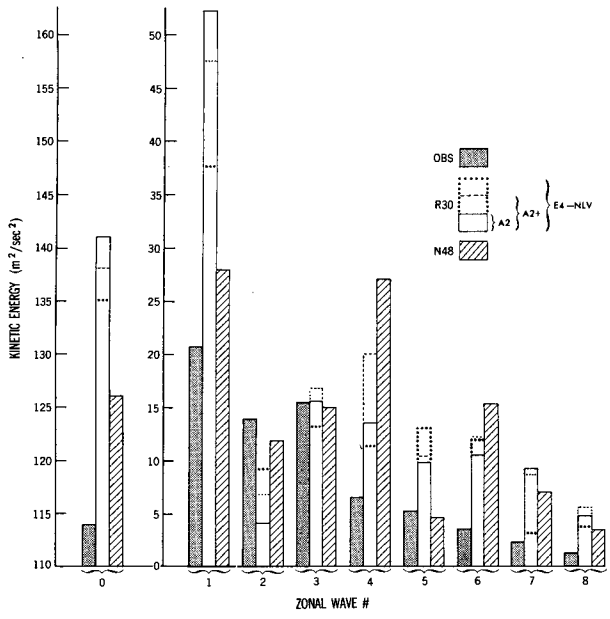

FIG. 16. Day 6–15 time means of the instantaneous R30A2, R30A2+, R30E4-NLV, N48 and observed Fourier spectra of kinetic energy for the 1 January 1977 case and the 34–55°N extratropics belt. Units are $m^2\ s^{-2}$. Ordinate scale is linear.

wavenumber modes. A comparison of the various spectra essentially corroborates the subjective map results that the planetary scale waves are sensitive to the horizontal and vertical dissipation. The R30A2 spectral variance is very excessive in wavenumbers $m = 0$ and 1 and very deficient in wavenumber $m = 2$, as is the R30A2-NLV (not shown). When stronger ∇^4 horizontal diffusion or especially E4 vertical diffusion is applied, the predicted spectral kinetic energy of the zonal mean flow and planetary scale waves agrees more closely with observation. More specifically, reductions occur in wavenumber 0 and 1 contributing to a 10% reduction in total kinetic energy, whereas the kinetic energy of wavenumber 2 increases somewhat. The redistribution of kinetic energy among zonal wavenumbers $m = 3$ to 8 is more irregular. But the total R30E4 kinetic energy within this spectral interval tends to be less excessive than the R30A2. The same holds for the kinetic energy spectra of the day 6–15 time mean flows (not shown).

Predicted and observed enstrophy spectra at 500 mb are plotted versus zonal wavenumber for the 34–55°N extratropics belt (Fig. 17) and the 1–19°N tropics belt (Fig. 18). The logarithmic abscissa and ordinate scales highlight the slopes of the spectra. In the extratropics, the slope $(d\epsilon/dm)_{\mathrm{R30A2}}$ is flatter than -1, whereas $(d\epsilon/dm)_{\mathrm{R30A2+}} \sim -1$. This result indicates the sensitivity of $d\epsilon/dm$ to the ν_{∇^4} horizontal diffusion coefficient and provides further evidence that the R30A2 model is underdamped. Incidentally, nonlinear horizontal diffusion ($k_0 = 0.20$) or E4 vertical diffusion had little effect upon the enstrophy spectrum at 500 mb.

Near the cutoff zonal wavenumber $m = m_{\max}$, $d\epsilon/dm$ is also sensitive to rhomboidal versus triangular truncation. Consider the Legendre transform

$$\zeta_{(m)}(\varphi) = \sum_{n=|m|}^{R^*} P_n^m(\varphi)\zeta_n^m, \tag{4}$$

where P_n^m is an associated Legendre polynomial of degree n and rank m and ζ_n^m is the corresponding spectral coefficient. The point is that $R^* = m_{\max} + |m|$ for rhomboidal truncation compared to $R^* = m_{\max}$ for triangular truncation. Thus, when $m = m_{\max}$, $m_{\max}$ spectral coefficients contribute to the Fourier coefficient $\zeta_{(m)}$ in the rhomboidal case whereas only 1 coefficient does so in the triangular case. Furthermore, calculations of $\tau_d(n)$ from Eq. (1) reveal that many of the components $\zeta_n^{m_{\max}}$, $n = m_{\max}, \cdots 2m_{\max}$, which contribute to $\zeta_{(m_{\max})}$ in the rhomboidal case are only weakly damped by moderate ∇^4 horizontal diffusion. Therefore, unless the terms in Eq. (4) fortuitously cancel, $|\zeta_{(m_{\max})}|^2$ should be relatively large. Not surprisingly, the slope $(d\epsilon/dm)_{\mathrm{R30A2}}$ near $m = 30$ steepened to approximately -1.3, when the R30A2 Fourier enstrophy spectrum was recalculated, ignoring all spectral components ζ_n^m, $n > 30$, which would have been discarded in a triangular T30 spectral representation.

In the tropics (Fig. 18), the observed (NMC-analyzed) enstrophy spectrum falls off quite steeply with

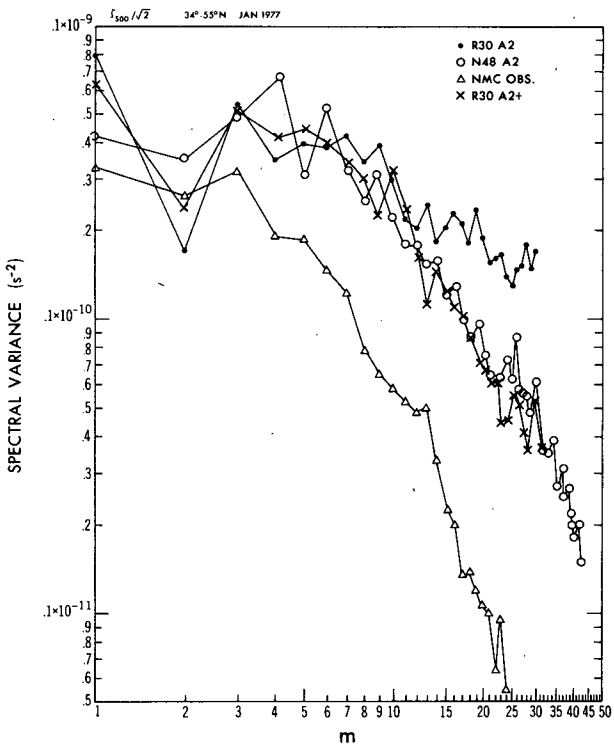

FIG. 17. Day 6–15 time means of the instantaneous R30A2, R30A2+, N48 and observed Fourier spectra of enstrophy vs zonal wavenumber for the 1 January 1977 case and the 34–55°N extratropics belt. Units are s^{-2}. Abscissa and ordinate scales are logarithmic.

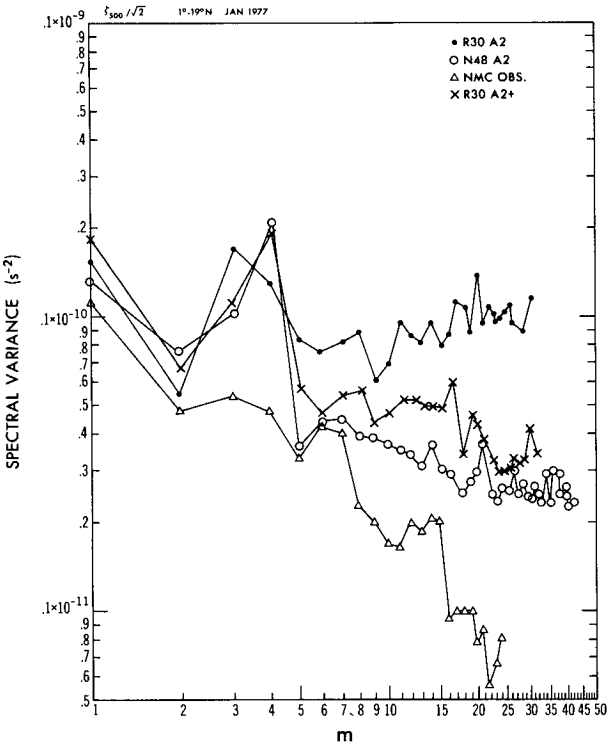

FIG. 18. As in Fig. 17 except for the 1–19°N tropics belt.

zonal wavenumber. Whereas the N48 enstrophy spectrum is almost flat at high wavenumbers, the R30A2 spectrum actually slopes upward, slightly. Moreover, the R30A2 spectrum contains approximately 300% more variance than the N48 in the wavenumber band $20 \leqslant m \leqslant 30$. Meanwhile, the R30A2+ enstrophy spectrum bears closest resemblance to the N48 spectrum (although the resemblance is not as striking in the tropics as at midlatitudes).

The shape of the predicted enstrophy spectra is presumably influenced by generation and dissipation terms as well as by nonlinear interaction terms. In convective regions of the tropics, the scenario discussed by Sardeshmukh (1982) for the Indian monsoon region, may be relevant. In his R15 GCM simulation, the Indian monsoon depression intensified rapidly, due to moist convection, i.e., the release of latent heat. His local vorticity budget revealed a simultaneous generation of anticyclonic vorticity above the level of latent heat release and cyclonic vorticity below it, consistent with divergent outflow and convergent inflow, respectively. In our R30 prediction, the tropical convection is longitudinally variable and noisy, as suggested by the time mean R30 precipitation field (see Appendix, Fig. A5). Thus, the predicted spectrum of enstrophy generation could be fairly flat at intermediate and high wavenumbers. Meanwhile, within the extratropics *in situ* baroclinic instability is probably a more important source of vorticity, particularly at intermediate length scales. Given underdamped conditions, higher as well as lower wavenumber components could be adversely affected viz. nonlinear transfer.

The enstrophy balances corresponding to the various model forecasts have not been computed. However, we have calculated the contributions of E4 and A2 vertical diffusion and ∇^4 and nonlinear horizontal diffusion to the spectral vorticity and temperature tendencies, i.e., $\partial\zeta/\partial t$ and $\partial T/\partial t$, from observed meteorological fields. For this purpose, the relevant R30L09 spectral models were integrated for one time step from observed monthly mean initial conditions. The latter were constructed from the daily NMC Flattery analyses of January 1977. This approach has two advantages: i) each diffusion term acts upon the same wind and temperature fields; ii) those fields are uncontaminated by forecast errors and model biases.

Spectral amplitudes of the appropriate A2 or E4 vertical diffusion terms and ∇^4 or nonlinear (NLV) horizontal diffusion terms have been contoured in spectral phase space. The contributions to $\partial T_8/\partial t$ and $\partial\zeta_8/\partial t$ are illustrated in Figs. 19 and 20. Here the subscript 8 denotes sigma level 8 ($\sigma_8 \sim 0.926$), which resides in the planetary boundary layer. The A2 and E4 vertical diffusion at 500 mb (not shown) would be negligible. Each panel in Figs. 19 or 20 corresponds to a particular diffusion term. Also, m is the zonal wavenumber, whereas j is the meridional wavenumber ($j = n - m$).

Inspection of Fig. 19 reveals that the A2 thermal diffusion term (upper left panel), i.e., dry convective adjustment, is relatively noisy, but weak. In contrast, the E4 diffusion term (lower left panel) is much stronger at lower wavenumbers, where the spectral amplitude of T_8 itself (not shown) is concentrated and tapers off more gradually than T_8. In principle, if the E4 term could be expressed as $-K_{E4}(m, j \cdots)T$, where the effective Newtonian damping coefficient K_{E4} would increase with wavenumber. Meanwhile, the highly scale selective ∇^4 horizontal thermal diffusion (upper right panel) is concentrated in the high wavenumber region. Note that the contour maps for strong ∇^4 diffusion would look identical except for a normalization factor, which is equal to the ratio of the strong versus standard diffusivities. Finally, the NLV term (lower right panel) is weaker overall (except at extremely low wavenumbers) and less scale selective than the ∇^4. This term is somewhat larger at sigma level 5 (not shown) where the wind shear is stronger.

In Fig. 20, the discrepancy between the A2 and E4 vorticity diffusion terms is quite dramatic. The A2 diffusion affects predominantly low to moderate wavenumber modes, tapering off at roughly the same rate as the vorticity (not shown) itself. In contrast, the E4 diffusion is concentrated in the high wavenumber modes and is comparatively less noisy. Thus, the effective Newtonian damping coefficient is not very dependent on wavenumber for A2 diffusion whereas it increases with zonal wavenumber for E4. The ∇^4 diffusion of vorticity is concentrated in the high two di-

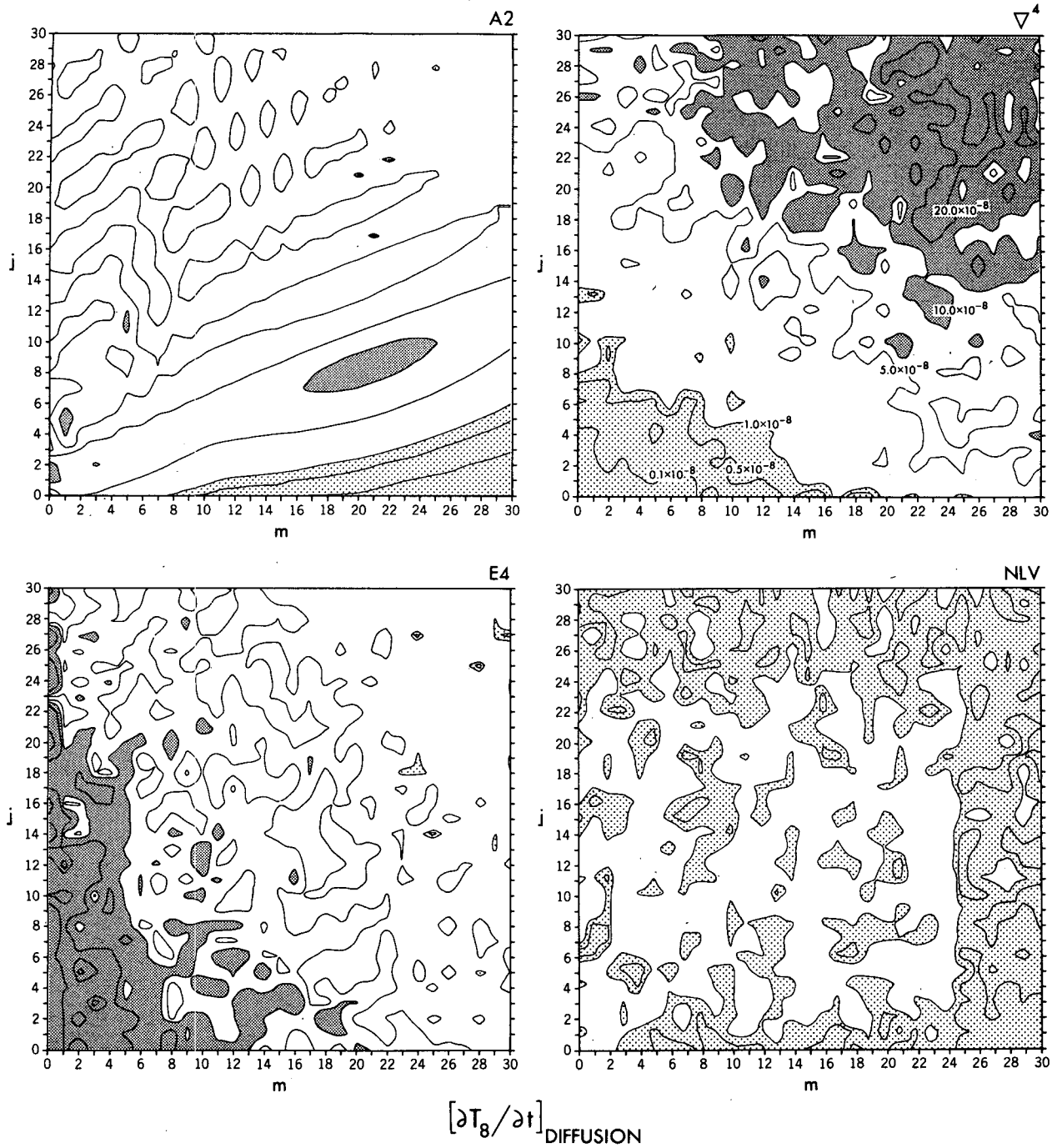

FIG. 19. Spectral amplitudes of thermal diffusion terms in the temperature tendency equation contoured as functions of zonal (m) and meridional (j) wavenumbers. Vertical diffusion: A2 (upper left) and E4 (lower left); horizonal diffusion: ∇^4 (upper right) and nonlinear (lower right) at sigma level 8. Shading where amplitude $> 1.0 \times 10^{-7}$ k s^{-1}; stippling where $<1.0 \times 10^{-8}$ k s^{-1}. R30L09 models were integrated for one time step from NMC January 1977 monthly mean initial conditions.

mensional wavenumber modes. However, there is now a sharp cutoff at zonal wavenumber 24, since only a negligible amount of enstrophy "leaks" into modes 25 to 30. The NLV term is somewhat weaker for ζ than for T at low wavenumbers, while the converse is true at intermediate to high wavenumbers.

The contribution of diffusion terms to the kinetic energy tendency was not calculated. However, we speculate that the E4 diffusion of the observed kinetic energy may attain its maximum value in the low wavenumber regions of the spectrum and that the A2 dissipation of observed kinetic energy should exceed the

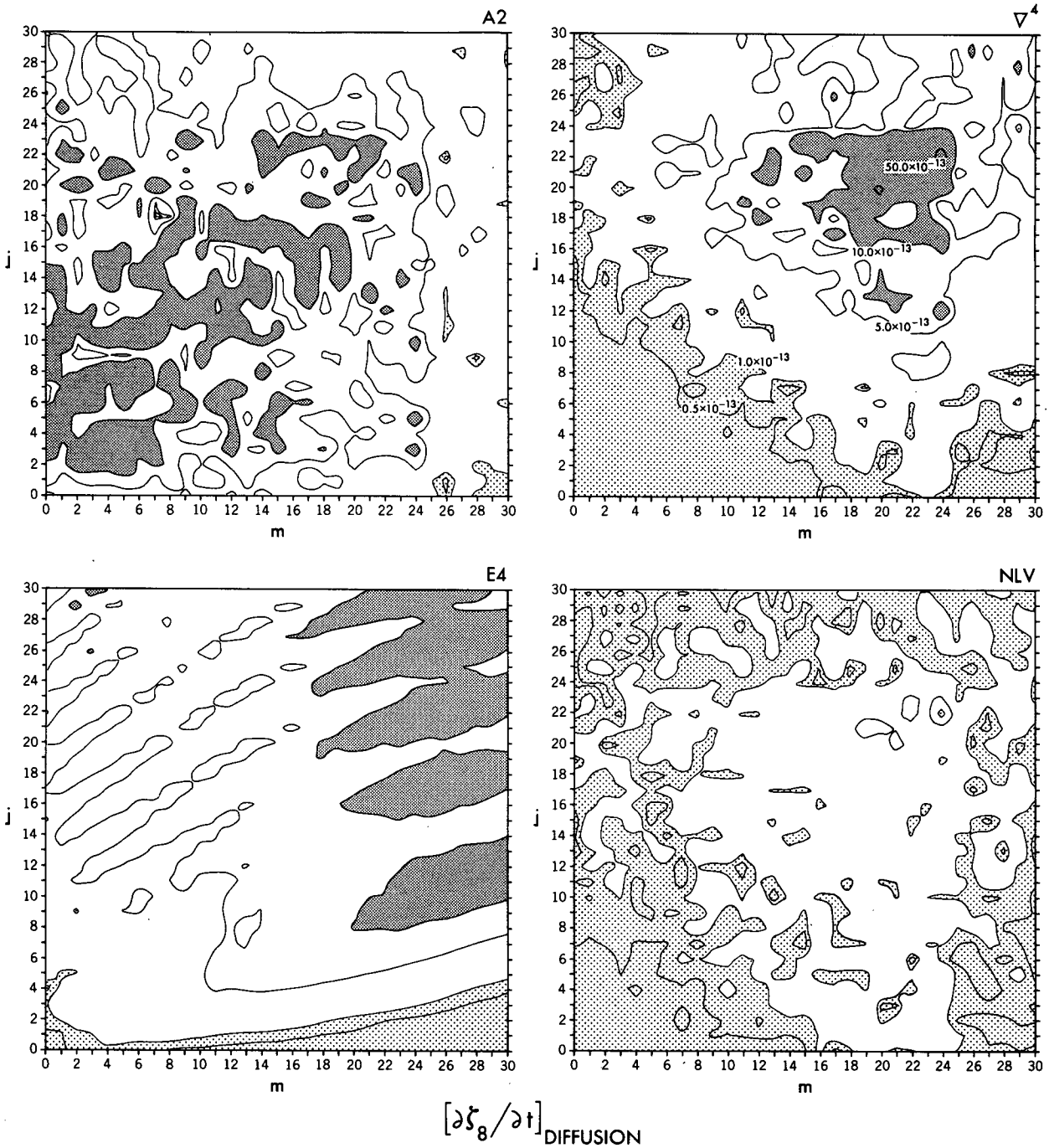

FIG. 20. As in Fig. 19 except for spectral amplitudes of vorticity diffusion terms in the vorticity tendency equation. Shading where amplitude $> 1.0 \times 10^{-12}$ s^{-2}; stippling where $< 1.0 \times 10^{-13}$ s^{-2}.

E4 dissipation, for low wavenumbers. In support of the first speculation: i) the E4 thermal diffusion is maximum for low wavenumbers (Fig. 19); ii) the dissipation of the available potential energy should be roughly proportional to the dissipation of the thermal variance; and iii) the kinetic energy and available potential energy spectra should have similar slopes according to the quasi-geostrophic turbulence theory of Charney (1971). Meanwhile the second speculation may be inferred from results for vorticity diffusion (Fig. 20), assuming that kinetic energy spectra have much steeper slopes than corresponding enstrophy spectra.

In short, we may infer that the A2 dissipation rates of available potential and kinetic energy have sub-

stantially different spectral distributions. This is apparently not true, however, for the corresponding E4 dissipation rates. Also, the E4 vertical mixing should be locally more intense than A2, where it is needed most, i.e., in regions where the Richardson number is negative or only weakly positive. In any case, the weak A2 thermal dissipation could conceivably promote the accelerated development of transient baroclinic disturbances. Conversely, inclusion of Prandtl thermal vertical mixing could lead to excessive eddy damping. Intriguingly, Miyakoda and Sirutis (personal communication, 1983) find that N48A2 solutions possess more transient (but less stationary) eddy kinetic energy than analogous N48E4 solutions.

Incidentally, some results of turbulence cascade experiments performed in the *inviscid limit,* appear to lend credence to the hypothesis that our R30L09 *A2* GCM is underdamped. For example, using a moderately high resolution inviscid, barotropic model, Basdevant and Sadourny (1975) found that their energy cascade proceeded to the gravest modes. Simultaneously, the enstrophy tended towards a state of equipartition in the tail of the spectrum. Meanwhile, Rhines (1975) pointed out that diffusion as well as β (the derivative of the Coriolis parameter) can inhibit the energy cascade. There are some caveats, however. First, the numerical models used to perform turbulence cascade experiments are highly idealized, i.e., have only 1 or 2 vertical levels and lack planetary boundary layers, moist convection, orography, etc. Also the initial conditions, imposed forcing and length of integration, are quite different than in our case.

According to Rhines (1975) and Williams (1979), the surface drag can weaken the energy cascade to lower wavenumbers and the enstrophy cascade to higher wavenumbers in a 2 level model. Although the direct influence of surface drag upon the free atmosphere should be greatly diminished in a 9 level model, the planetary boundary layer processes could serve as an intermediate link. Indeed, in our R30 integrations, the vertical diffusion processes bore most of the burden of dissipating large to intermediate scale disturbances. Thus, further refinement of the parameterization of subgrid-scale vertical mixing would appear to be a worthwhile endeavor.

Nonetheless, the horizontal dissipation of intermediate scale disturbances could perhaps be more finely tuned for the extended range prediction problem in which the diabatic forcing and dissipation are approaching a state of quasi-stationary balance. The requirements may be different than for the short range, when the development of first generation baroclinic-synoptic scale disturbances is of key concern.

6. Concluding remarks

The main objective of the present paper was to demonstrate the viability of the GFDL R30L09 "A" spectral model at medium range prediction. Three winter blocking cases were considered. Forecasts by the analogous N48L09 "A" grid point model provided a standard of comparison. A second objective was to examine the role of insufficient frictional dissipation upon the development of an overly symmetric midlatitude circulation.

Attention was focussed upon the medium range deterministic and day 5–15 time mean forecasts of geopotential height. In all three cases, the R30 and N48 forecasts possessed at least a residual level of skill. However, their quality was more case-dependent than spectral versus grid point model-dependent. Overall, the spectral model forecasts appeared to verify nearly as well as the more costly grid point model forecasts. The case of 16 January 1979 was the most successful. Here, both models simulated the persistence, if not the intensity, of the Atlantic block. Beyond day 10 the R30 simulation of the block was somewhat more realistic than the N48.

For the 5–10 day forecast range and the eastern Pacific–North American sector, R30 transients in January 1977 and R30 and N48 transients in January 1979 could apparently be identified with observed transients. Although the predicted transients tended to propagate too rapidly across the United States, they were retarded as they approached the east coast by a well established Atlantic blocking ridge. In this manner, a well-simulated blocking ridge may help to control the phase errors of upstream transient disturbances and to maintain a 1 to 1 correspondence between predicted versus observed transients upstream of the block.

The amplitude of N48L09 as well as R30L09 "A2"–predicted cutoff lows and troughs tended to become substantially weaker than observation rather rapidly. In the case of 1 January 1977, however, the R30L09 "A2" planetary scale waves became noticeably more deficient in amplitude than the N48L09 "A2". The R30L09 medium range forecast results suggested that the amplitude of the quasi-stationary planetary waves is affected by the horizontal diffusion. Also, in diffusion sensitivity experiments performed for the 1 January 1977 case, stronger ∇^4 horizontal diffusion ($\nu_{\nabla^4} \sim 1.0 \times 10^{16}$ m^4 s^{-1}) and especially E4 vertical diffusion retarded the decay of the predicted quasi-stationary planetary waves and favorably altered the spectral distribution of kinetic energy. The stronger ∇^4 horizontal diffusion considerably steepened the slope of the extratropical enstrophy spectrum and reduced the amount of enstrophy in the tropics. Further analysis indicated that the thermal diffusion in the low to moderate wave number regime is disproportionately weak in the R30L09 "A2" as compared to the R30L09 "E4" model. The *A2 thermal* vertical diffusion could presumably be enhanced by restoring Prandtl thermal mixing. However, the E4 formulation is theoretically more sound and appears to have a favorable influence. A detailed multi-case study of various physics param-

eterization, including "A2", "E4" and "F3" ("E4" plus the Arakawa–Schubert cumulus parameterization) is being carried out by Miyakoda and Sirutis (personal communication, 1983).

To date, one integration of a high resolution, i.e., R60L09 "A2" hemispheric spectral model has been attempted, from 1 January 1977 initial conditions. Here, weak ∇^4 horizontal diffusion ($\nu_{\nabla^4} \sim 5 \times 10^{14}$ $m^4 s^{-1}$) may have contributed to the zonally symmetric character of the resulting 10 day forecast. Extended range integrations are planned at GFDL using an R42L18 "F3" global spectral model. We believe that improved diffusion schemes and/or diffusion coefficients may be important for the zonal mean bias problem in high resolution models such as the above. Also, recent work by J. M. Wallace *et al.* (1983) suggests that the proper treatment of orography may be even more important. Perhaps a north–south oriented mountain barrier may be better able to selectively retard or divert the impinging zonal flow component than ∇^4, E4 or nonlinear diffusion.

Acknowledgments. We are most grateful to Dr. J. D. Mahlman for his valuable input concerning the dissipation of transient, baroclinic disturbances and the possible influence of the local mean flow upon the propagation speed of such disturbances. Also, discussions with Dr. G. P. Williams on the kinetic energy cascade were very useful. Drs. J. D. Mahlman, N-G. Lau and K. Miyakoda painstakingly reviewed the manuscript and offered many constructive suggestions. Mr. J. Sirutis carried out the integrations of the N48L09 grid point model and kindly supplied us with history tapes of the forecast results. The manuscript was typed by Ms. Betty Williams. The figures were drafted by Messrs. P. Tunison and W. Ellis and photographed by Mr. J. Conner.

APPENDIX

General Circulation for the 1 January 1977 Case

The predicted, medium range general circulation of a representative case is probably of sufficient interest to some readers to warrant the following discussion. Day 5–15 time means of selected R30 and N48-predicted and observed fields for the 1 January 1977 case are compared below. That case verified second best of three cases on the basis of anomaly correlation coefficients (see Fig. 7). Corresponding results for the 1 March 1965 and 16 January 1979 (not shown) are roughly comparable in overall quality. Since the forecast range is 1 to 2 weeks, the predicted time mean general circulation is likely to be influenced by the initial conditions (Shukla, 1981) and predictability decay as well as model bias. Certain model biases for this forecast range may be more evident than others. Whether they would exist in the model's climatological mean solution could only be ascertained by performing much longer integrations. But such an endeavor is beyond the scope of the present study.

Cross sections of the observed time mean temperature field as well as the R30 and N48 predicted temperature anomaly $\langle \overline{\Delta T} \rangle$ are plotted in Fig. A1. The R30 and N48 results are qualitatively similar. Cold anomalies are found in the middle and upper troposphere between 50°S and 70°N and warm anomalies in the tropics and subtropics near the surface. The N48 and especially the R30 north polar tropospheres are much too cold.

The R30 and N48 zonal wind cross sections $\langle \bar{u} \rangle$ for January 1977 (Fig. A2) agree qualitatively with observation and resemble each other. The predicted tropospheric jet cores in the northern hemisphere are centered slightly north of the observed core and are somewhat weaker. The predicted tropical easterlies extend throughout the vertical column, in disagreement with observation. Similarly, as expected, the latitude boundaries and intensities of the predicted polar easterlies differ somewhat from observation.

The $\langle \bar{v} \rangle$ and $\langle \bar{\omega} \rangle$ components of the predicted time mean meridional circulation are shown in Fig. A3 and Fig. A4, respectively. For the most part, the R30 and N48 results are rather similar to each other, except that the N48 vertical motion in the ascending branch of the tropical Hadley cell is more intense. Unfortunately, the only readily available verification, i.e., the NMC Hough analyses had essentially nondivergent winds. Meanwhile, Rosen and Salstein's (1980) analysis of the mean meridional mass stream function for December 1976–February 1977, based upon rawinsonde data, indicates a somewhat weaker meridional circulation. However, their 90 day averaging period and the paucity of tropical rawinsonde observations (Oort, 1978) could be contributing factors.

Global maps of the predicted precipitation fields, as well as a seasonal climatology obtained from Miyakoda (personal communication, 1980) are displayed in Fig. A5. In the tropics, the N48 ITCZ is somewhat more intense and has more continuity in longitude than the R30. In this respect, the N48 result is in better agreement with climatology. Furthermore, the N48 tropical convective precipitation is somewhat more noisy than the R30. The above results are perhaps a consequence of the finer horizontal resolution of the N48 model.

Meanwhile, in the extratropics, the R30 precipitation is more noisy and more intense than the N48 or climatology, especially over Siberia. The relatively finer resolution of the R30 model may be invoked at high latitudes as a contributing factor. However, perhaps more importantly, erroneous supersaturation occurs in regions of low water vapor content due to spectral truncation. Prior to truncation, the local relative humidity is bounded by the condensation criterion, i.e., 80% for large scale condensation and convective ad-

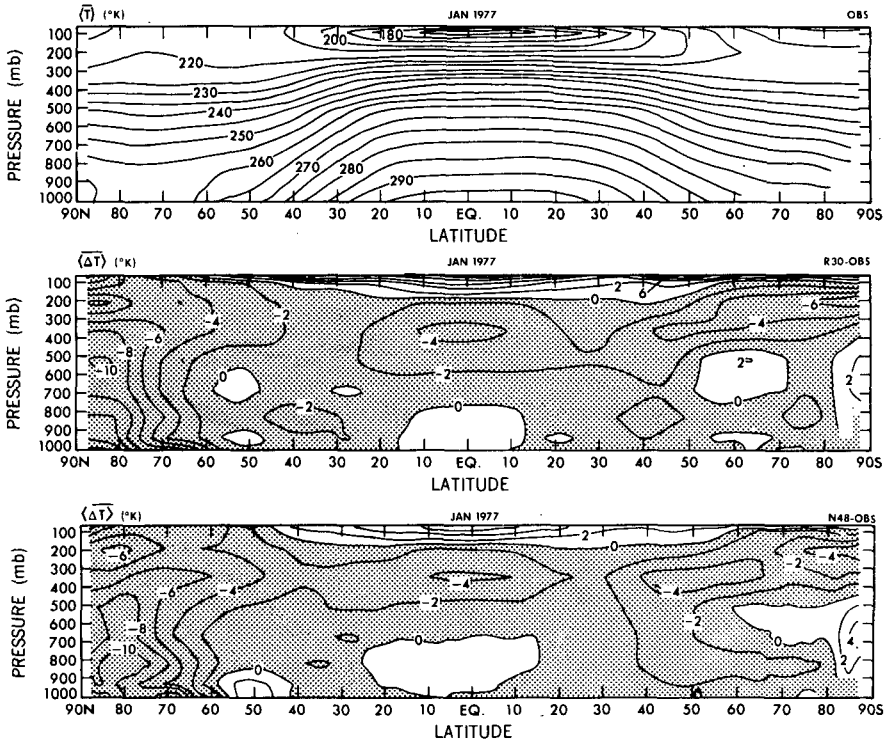

FIG. A1. Global latitude–height cross sections of observed, day 5–15 time mean temperature (top), and of R30L09 (center) and N48L09 (bottom) temperature errors for the 1 January 1977 case. Contour interval is 5 K for observation and 2 K for forecast errors. The latter are negative in stippled regions.

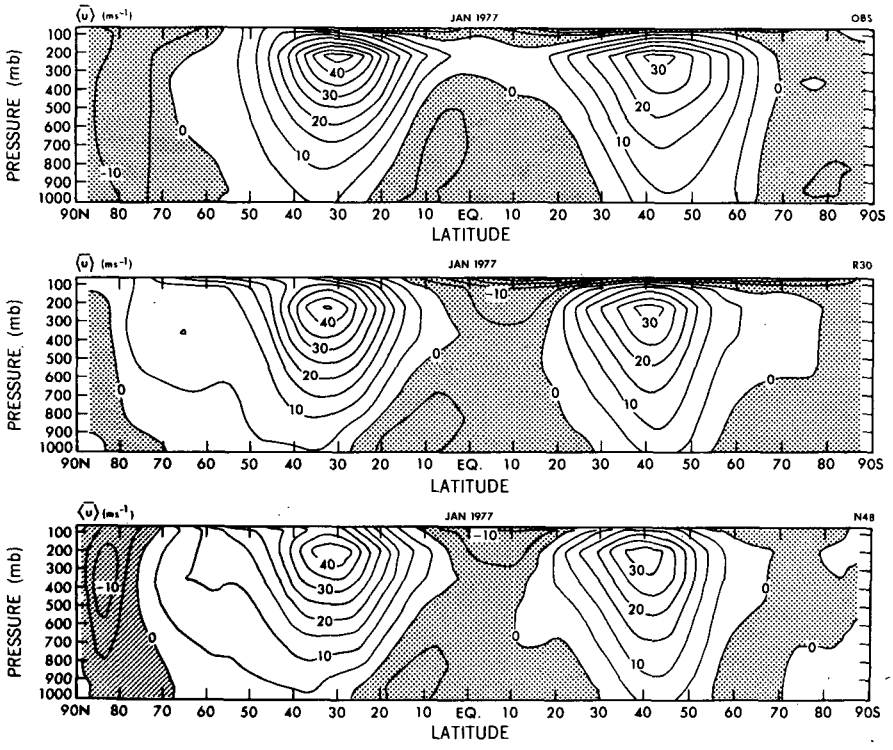

FIG. A2. Global latitude–height cross sections of the day 5–15 time mean observed (top), R30L09 (center) and N48L09 (bottom) zonal wind for the 1 January 1977 case. Contour interval is 5 m s^{-1}. Flow is easterly in stippled regions.

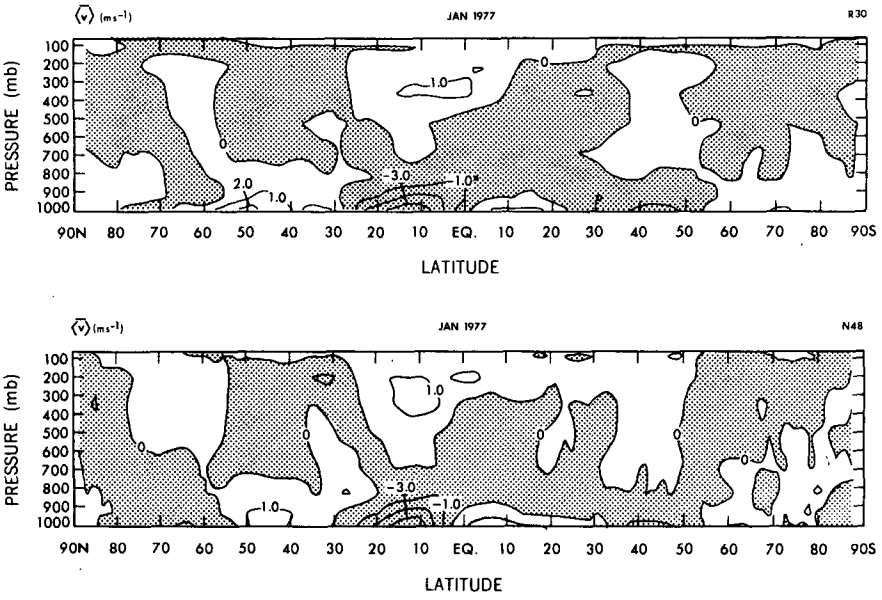

FIG. A3. As in Fig. A2, except for meridional wind component. Contour interval is 1 m s^{-1}. Flow is northerly in stippled regions.

justment. But after spectral truncation, it can exceed 100% or even 110% locally at subpolar and polar latitudes. Consequently, some extra precipitation may be induced, locally, during the next time step. This precipitation is irreversible and the generation of negative mixing ratios at other longitudes due to spectral truncation does not provide direct compensation. Perhaps the degree of supersaturation could be reduced if negative borrowing (see GS) were supplemented by local grid point smoothing of the water vapor field just prior to large scale condensation–convective adjustment.

Incidentally, some discrepancies between the day 5–15 time mean prediction and seasonal climatology are legitimate. In particular, the R30 and N48 precipitation bands off the east coast of the United States in January 1977 are consistent with the observed cyclonic activity in this region.

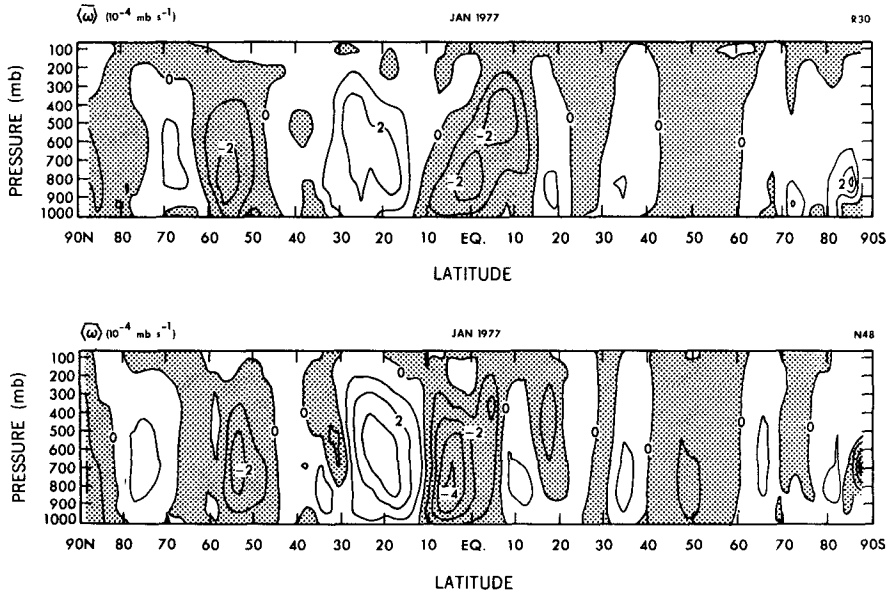

FIG. A4. As in Fig. A2 except for pressure vertical velocity. Contour interval is 1.0×10^{-4} m s^{-1}. Vertical motion is upward in stippled regions.

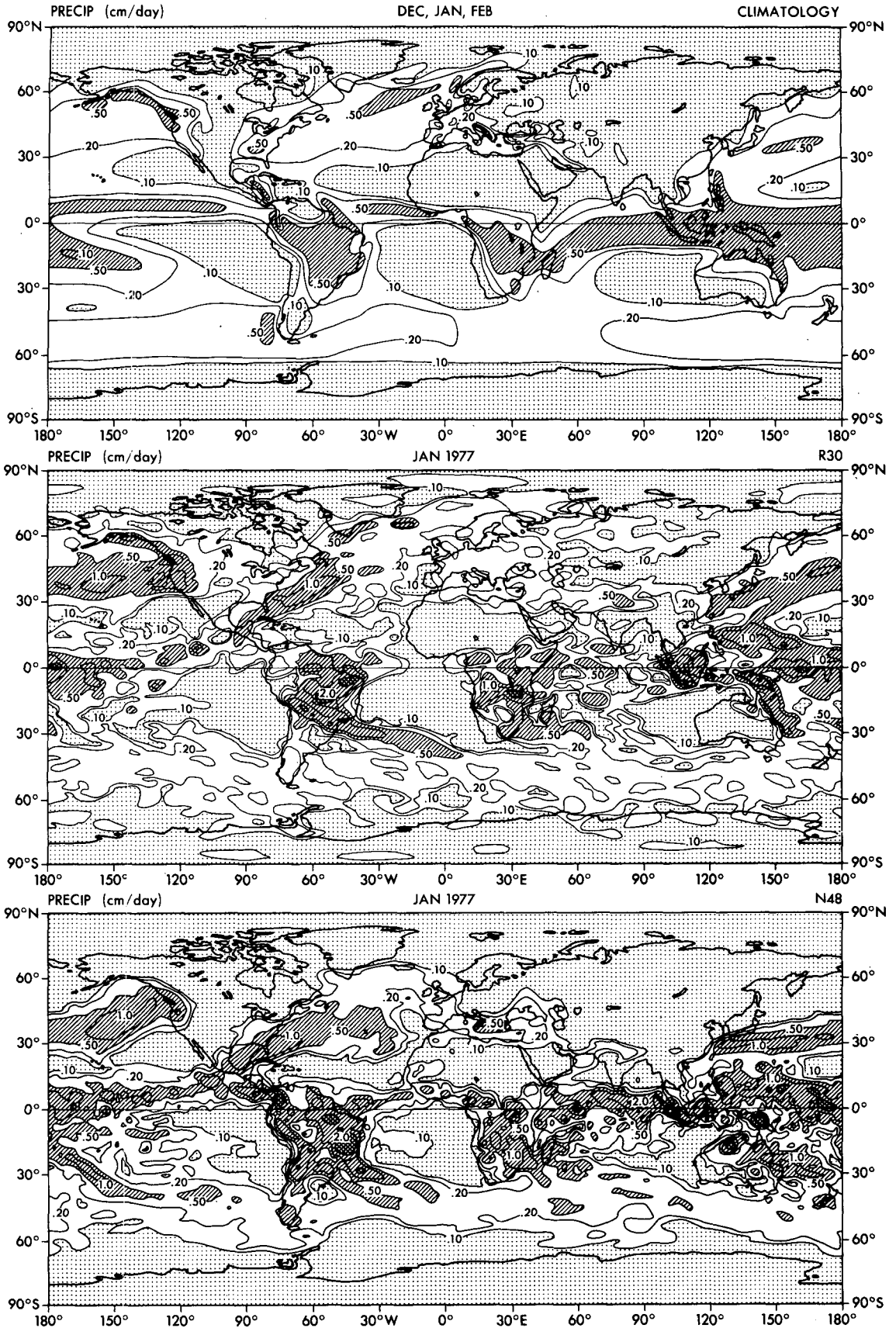

FIG. A5. Global maps of day 5–15 time mean precipitation rate r_p for the 1 January 1977 case. Winter climatology (top), R30L09 forecast (center), N48L09 forecast (bottom). $r_p \leq 0.1$ (sparsely shaded), $0.1 < r_p \leq 0.5$ (unshaded), $0.5 < r_p \leq 2.0$ (hatched), and $2.0 < r_p$ (cross-hatched) cm day^{-1}.

REFERENCES

Baede, A. P. M., A. W. Hansen, 1977: A ten-day high-resolution nonadiabatic spectral integration: A comparative study. Tech. Rep. No. 7, European Centre for Medium Range Weather Forecasts, 82 pp.

Basdevant, C., and R. Sadourny, 1975: Ergodic properties of inviscid truncated models of two-dimensional incompressible flows. *J. Fluid Mech.*, **69,** 673–688.

Bengtsson, L., 1981: Numerical prediction of atmospheric blocking—A case study. *Tellus,* **33,** 19–42.

Brown, J. A., Jr., and K. A. Compana, 1978: An economical time-differencing system for numerical weather prediction. *Mon. Wea. Rev.*, **106,** 1125–1136.

Charney, J. G., 1971: Geostrophic turbulence. *J. Atmos. Sci.*, **28,** 1087–1095.

Fels, S. B., and M. D. Schwarzkopf, 1975: The simplified exchange approximation: A new method for radiative transfer calculation. *J. Atmos. Sci.*, **32,** 1475–1488.

Flattery, T. W., 1971: Spectral models for global analysis and forecasting. *Proc. Sixth AWS Tech. Exch. Conf.*, U.S. Naval Academy, Environmental and Technical Applications Center, Scott Air Force Base, IL 62225. Air Weather Service Tech. Rep. 242, 42–54.

Gordon, C. T., and W. F. Stern, 1982: A description of the GFDL global spectral model. *Mon. Wea. Rev.*, **110,** 625–644.

——, L. Umscheid Jr. and K. Miyakoda, 1972: Simulation experiments for determining wind data requirements in the tropics. *J. Atmos. Sci.*, **29,** 1064–1075.

Hollingsworth, A., K. Arpe, M. Tiedtke, M. Capaldo and H. Savijärvi, 1980: The performance of a medium-range forecast model in winter: Impact of physical parameterization. *Mon. Wea. Rev.*, **108,** 1736–1773.

Jarroud, M., C. Girad and U. Cubasch, 1981: Comparison of medium range forecasts made with models using spectral or finite difference techniques in the horizontal. Tech. Rep. No. 23, European Centre for Medium Range Weather Forecasts, 96 pp.

Kurihara, Y., 1965: Numerical integration of the primitive equations on a spherical grid. *Mon. Wea. Rev.*, **93,** 399–415.

Manabe, S., and R. F. Strickler, 1964: Thermal equilibrium of the atmosphere with a convective adjustment. *J. Atmos. Sci.*, **21,** 361–385.

Mellor, G. L., and T. Yamada, 1974: A hierarchy of turbulence closure models for planetary boundary layers. *J. Atmos. Sci.*, **31,** 1791–1806.

Miyakoda, K., G. D. Hembree, R. F. Strickler and I. Shulman, 1972: Cumulative results of extended forecast experiments, I. Model performance for winter cases. *Mon. Wea. Rev.*, **100,** 836–855.

——, —— and ——, 1979: Cumulative results of extended forecast experiments. II: Model performance for summer cases. *Mon. Wea. Rev.*, **107,** 395–420.

——, C. T. Gordon, R. Caverly, W. Stern, J. Sirutis and W. Bourke, 1983: Simulation of a blocking event in January 1977. *Mon. Wea. Rev.*, **111,** 846–869.

Namias, J., 1978: Multiple causes of the North American abnormal winter 1976–77. *Mon. Wea. Rev.*, **106,** 279–295.

Oort, A. H., 1978: Adequacy of the rawinsonde network for global circulation studies tested through numerical model output. *Mon. Wea. Rev.*, **106,** 174–195.

Ploshay, J. J., R. K. White and K. Miyakoda, 1983: FGGE level III-B daily global analyses, Part I (Dec. 1978–Feb. 1979). NOAA Data Rep. ERL GFDL-1. GFDL, Princeton, 278 pp.

Rhines, P. B., 1975: Waves and turbulence on a β plane. *J. Fluid. Mech.*, **69,** 417–443.

Rosen, R. D., and D. A. Salstein, 1980: A comparison between circulation statistics computed from conventional data and NMC Hough analyses. *Mon Wea. Rev.*, **108,** 1226–1247.

Sardeshmukh, P., 1982: Mechanisms of monsoonal cyclogenesis, Ph.D. thesis, Princeton University, Geophysical Fluid Dynamics Laboratory, 192 pp.

Shukla, J., 1981: Dynamical predictability of monthly means. *J. Atmos. Sci.*, **38,** 2547–2572.

Smagorinsky, J., S. Manabe and J. L. Holloway, Jr., 1965: Numerical results from a nine-level general circulation model of the atmosphere. *Mon. Wea. Rev.*, **93,** 727–798.

Somerville, R. C. J., 1980: Tropical influences on the predictability of ultra long waves. *J. Atmos. Sci.*, **37,** 1141–1156.

Umscheid, L., Jr., and M. Sankar-Rao, 1971: Further tests of a grid system for global numerical prediction. *Mon. Wea. Rev.*, **99,** 686–690.

Wallace, J. M., S. Tibaldi and A. J. Simmons, 1983: Reduction of systematic forecast errors in the ECMWF model through the introduction of an envelope orography. *Quart. J. Roy. Meteor. Soc.*, **109,** 673–717.

Williams, G. P., 1979: Planetary circulations: III. The terrestrial quasi-geostrophic regime. *J. Atmos. Sci.*, **36,** 1409–1435.

Williamson, D. L., 1981: Storm track representation and verification. *Tellus,* **33,** 513–530.